

PSFC/JA-09-20

**Feasibility Study for Employing
High Temperature Superconductor in a
Steady State
Compact Stellarator-Based Reactor Design**

L. Bromberg, P. Michael, J.V. Minervini, J.H. Schultz
MIT Plasma Science and Fusion Center

August 6, 2009

This work was sponsored by Princeton University Subcontract Award Number S00828F.

*Feasibility Study for Employing High Temperature Superconductor in a Steady State
Compact Stellarator-Based Reactor Design*

L. Bromberg, P. Michael, J.V. Minervini and J.H. Schultz

Prepared by the
Plasma Science and Fusion Center
Massachusetts Institute of Technology
Cambridge MA 02139

June 27 2009
Finalized July 16, 2009

Final report

Award Number: Subcontract No. S00828F
MIT Award Number : 016819-001

Abstract

The use of monolithic High Temperature Superconductors (HTS) for field shaping in stellarators and tokamaks is presented. Design issues relevant to stellarator magnets using single crystal or highly textured YBCO monoliths will be discussed. The excellent properties of YBCO operating at elevated temperatures (> 10 K) will be summarized. High field, cryo-stable, highly complex magnet field topologies can be generated using the techniques discussed in this paper. The diamagnetic properties of the bulk HTS material can be used to provide simple mechanisms for providing field-shaping. Engineering constraints, such as stresses in the superconducting monoliths, support, quench protection, superconducting stability of the monoliths and required external support structure will be described. The limitations imposed by different fusion environments on the performance and lifetime of the HTS monoliths will be reviewed, both for near term experiments as well as long term stellarator fusion reactors. Since the HTS monoliths require no insulation or copper for stability/quench protection, the typical irradiation limits on these elements are eliminated. Nuclear heating, due to the high temperature of operation of the HTS compounds, is also very much relaxed, since at 50 K it is possible to remove more than one order of magnitude higher cryogenic loads than at 4 K, for the same refrigerator power. In addition, irradiation damage limits on HTS, and YBCO in particular, are no lower than for Nb_3Sn .

Keywords-component; HTS bulk, monoliths, stellarator, magnetic field shaping

TABLE OF CONTENTS

I.	INTRODUCTION	5
II.	HTS MONOLITHS	5
A.	PROPERTIES AND AVAILABILITY	5
B.	MODELING OF HTS BULK.....	6
C.	ESTIMATE OF FORCES/CURRENTS IN HTS MONOLITH	7
D.	EFFECT OF GAPS BETWEEN MONOLITHS	8
E.	CHARGING/DISCHARGING THE MONOLITHS	8
III.	TOROIDAL FIELD RIPPLE CANCELLATION	11
A.	SINGLE LAYER OF MONOLITHS WITH 16 AZIMUTHAL MONOLITHS	13
B.	MULTIPLE LAYERS.....	13
C.	CURRENTS IN MONOLITHS	19
D.	DECREASED GAPS BETWEEN MONOLITHS	23
E.	DECREASED RADIAL GAPS BETWEEN ADJACENT LAYERS OF MONOLITHS	26
F.	VARIATION OF THE RADIAL LOCATION OF THE MONOLITHS	26
G.	MAGNETIC FIELD RIPPLE	28
	DISCUSSION.....	31
IV.	STELLARATOR GEOMETRY	36
V.	CHARGING AND FIELD CREEP.....	37
A.	EXPERIMENTAL ASSEMBLY.....	39
B.	MAGNETIC FIELD AS A FUNCTION OF TEMPERATURE	43
C.	MAGNETIC FIELD STABILITY AS FUNCTION OF TEMPERATURE OF OPERATION	44
D.	MAGNETIC FIELD UNIFORMITY	50
VI.	RADIATION DAMAGE OF HTS	52
	ACKNOWLEDGMENT	55
	REFERENCES	56

I. INTRODUCTION

Stellarators offer substantial physics advantages for fusion reactors, both near term as experimental facilities as well as long term as commercial fusion reactors. Stellarators do not have disruptions, they are truly steady state and have high beta limits that make them attractive, among others. On the other hand, engineering of stellarators is challenging, in particular, the design of the magnetic field coils and the diverter.

In this paper and its accompanying paper [Brown] a novel method is investigated to simplify the magnetic field coils. The use of monolithic High Temperature Superconductors (HTS) for field shaping in stellarators and tokamaks is presented. The basic concept investigated in this paper is to use a relatively simple coil set that generates a background magnetic field, and use monoliths of superconductor to shield/shape the magnetic field to the desired configuration.

The properties of presently monolithic HTS are described in section II, as well as the physical model used to describe the superconducting monoliths. YBCO has excellent properties operating at elevated temperatures (> 10 K). High field, cryo-stable, highly complex magnet field topologies can be generated using this material. The diamagnetic properties of the bulk HTS material can be used to provide simple mechanisms for providing field-shaping.

Section II describes the design issues relevant to stellarator magnets using single crystal or highly textured YBCO monoliths will be discussed. Engineering constraints, such as stresses in the superconducting monoliths, support, quench protection, superconducting stability of the monoliths and required external support structure will be described.

II. HTS MONOLITHS

A. *Properties and availability*

There is a small program worldwide to develop monoliths of HTS materials. During the initial phases of high temperature superconductivity, the only materials that were available were bulk

materials. This was the case for BSCCO 2212 and YBCO. Wires were initially made from 2212, but this effort was dropped because of the relatively poor superconducting properties at 77 K.

Presently, both 2212 and YBCO are available. 2212 is more developed, because of applications as current leads, and more recently, as components for fault current limiters. 2212 is available from Nexans, either as rods, cylinders or as plates. While its properties are lackluster at 77 K, they are very good at 20-30 K.

YBCO is being developed mainly as materials to be used in bearings, in the US (Boeing), Europe (Nexans) and Japan (ISTEC), among others. The characteristics of this material are nothing less than spectacular, at temperatures up to 60-65 K. YBCO has limited current density capabilities at 77 K, good enough for tapes, but not for high field magnet applications. They need to be subcooled.

The most impressive performance of YBCO pucks has been a 17 T magnet at 29 K without a background field. For 2212, the MIT group has built a 3 T magnet at 4 K, and a 1 T insert in a 19 T background [Bromberg, private communication].

These materials are available at costs of 15 €/cm² (150 k€/m²).

B. Modeling of HTS bulk

The interaction of the superconducting bulk material with magnetic fields is very non-linear and complex. In this section two methods that simplify the complex behavior is described. The methods will be used in the remaining of the document to analyze the interaction between tiles and the magnetic field.

Using the simple Bean model of superconductivity, the superconducting monoliths are assumed to be at critical current density. As the external field is raised, currents are generated on the surface of the monolith to prevent penetration of the field to the bulk. The current density is a function of the temperature of the monolith and the local applied field. The “skin” current thickness increases with increasing magnetic fields. As the field decreases, edge currents flow in the reverse direction on the surface, trapping locally some magnetic field.

If the current density capabilities of the monoliths is large and the thickness of the skin currents is small compared with the size of the monoliths, the monoliths can be described as “diamagnetic” elements.

Two methods have been used to describe the diamagnetic model of the HTS monoliths. The first one assumes that the magnetic field is parallel to all the surfaces of the monolith. The second one just assumed that magnetic permeability of the HTS monoliths is very small. While either method works, the second one is easier to implement, as applying the boundary conditions to the all the surfaces of the monoliths is time consuming.

We have used $\mu = 0.001$ in the remaining of this paper to describe the HTS monoliths.

C. Estimate of forces/currents in HTS monolith

The interaction between HTS monoliths and magnetic field can be divided into two effects. The first one are the surface currents that exclude the external magnetic field from the superconductor. It is straight forward to estimate the value of these currents. The surface current density excited by the presence of the field is simply

$$K = B_0/\mu_0$$

where B_0 magnetic field external to the surface of the monoliths. The critical current densities of YBCO are on the order of 10^9 - 10^{10} A/m². Thus, to expel a field of 5 T, the thickness of the current carrying layer It is expected that the value of the field outside of the surface of the monolith is comparable to the applied field, B_0 , (the assumption being that the main effect of the HTS monoliths is to “globally” turn the direction of the magnetic field. These currents exist even if the wide surface of the monolith is aligned with the magnetic field, and thus it is not expected to modify the direction of the field.

The second effect is due to the interception of fields perpendicular to the wide surface of the monolith. Assuming that the tiles have a typical dimension of a (diameter, or average diameter of the tiles), the magnetic moment generated by the presence of the monolith is

$$m \sim \pi^2/4 B_0 a^3 \cos(\delta) / \mu_0$$

where δ the angle between the main normal to the monolith and the applied magnetic field.

The main difficulty with these simple model arises because of the interaction with the adjacent tiles, which generate local magnetic fields. Thus, it is needed to solve the problem using multidimensional models.

The torque that a monolith will experience in the presence of a externally applied magnetic field B_o is on the order of

$$\tau = m \times B_o \sim \pi^2/4 B_o^2 a^3 \sin(\delta) \cos(\delta) / \mu_o$$

The forces/torques are very large, and need to be supported. In order to calculate the forces quantitatively, it is needed to calculate the full multidimensional effects.

D. Effect of gaps between monoliths

The magnetic field does not have to follow the main surface of the superconducting monoliths in the gaps between monoliths, that is, the magnetic field can “escape” through these regions.

One option to avoid the effect of the gaps between monoliths is to place multiple layers of monoliths, such that they are staggered. Although the field can escape through the gap, it is intercepted by the monolith behind.

The impact of the staggered layer of monoliths needs also to be calculated numerically. This is done in the next section.

E. Charging/discharging the monoliths

Using the Bean model (critical current density in the superconductor at all times), it is possible to construct the ideal charging/discharging of the monoliths. Figure 1 shows the cycle of charging and discharging.

At the top the region with applied magnetic field is shown, as well as a schematic of the monolith (in black). It is assumed that a uniform external field is applied to the monolith.

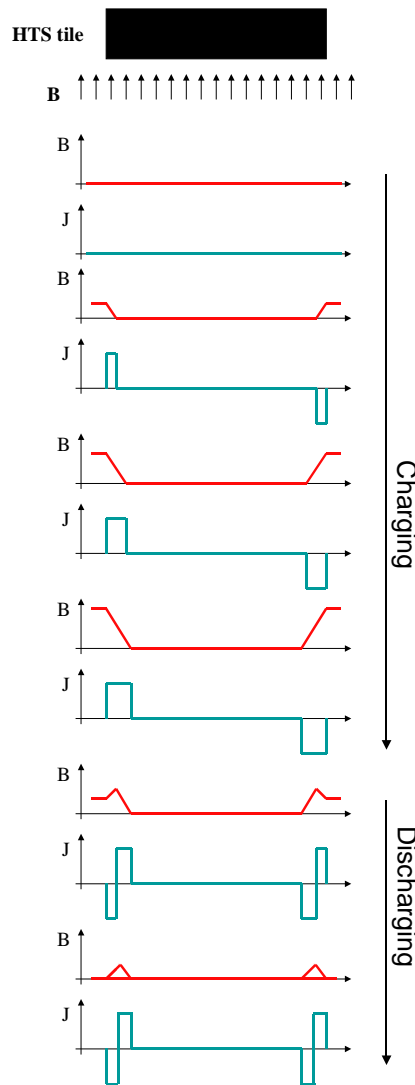


Figure 1. Schematic diagram of charging/discharging of the monoliths. Ideal case (no field creep)

At the beginning, there are no currents flowing in the monolith (cooled down to superconducting conditions in the absence of a magnetic field). As the field is increased (shown in the red line in the sequence of events in Fig. 1), the field penetrates to a depth that is determined by the current density at the critical condition at that magnetic field and that temperature. As the external applied field, the layer of current increases, with current that brings the superconductor to the critical condition. If the layer grows to be the size of the monolith, the field just penetrates through the entire monolith (and traps inside the monolith).

It should be noted that the field penetration results in heat dissipation in the superconductor. Because the field is penetrating, there is a loop voltage associated with the change in flux. The interaction of this voltage with the current results in dissipation. Monoliths are not particularly high thermal conductors, and for extreme applications (such as that of Tomita [Tomita] described in the next section, it is necessary to increase thermal conductivity in the superconductor.

When the field is reversed, the currents are not reduced to 0, as shown in Fig. 1. Instead, the current reverses in the outermost layer, preventing the change in flux in the interior of the monolith. As the field decreases further, the layer of reverse current increases, until the point where there is no external field. At this point the reverse current cancels the current increase during the charging period in the interior region. Although there is no field external to the monolith and in most of the interior, there is field trapped in the region in the periphery, as shown in the last period in Fig. 1.

In the application discussed here, it is best if the field does not penetrate fully the bulk material and instead remains in the periphery. It results in an easier problem to design, and is more reproducible.

III. TOROIDAL FIELD RIPPLE CANCELLATION

The quantitative work was complex. Simpler geometries were investigated and reported here. A simple geometry using helical coils for a cylindrical configuration proved to provide none of the simplifications that a 2D model would have. That is, the helical geometry still needs a 3D model for analysis.

The rest of the paper describes these calculations that are directly relevant to tokamaks [Boozer, Boozer1]. It is possible to build a simple 2D model where the monoliths are used for ripple control.

The simple model is shown in Fig. 1. The model uses a TF system with only 8 coils, with relatively large ripple. The coils are at 6 m, the ripple calculations in the following material are estimated at a radius of 4 m.

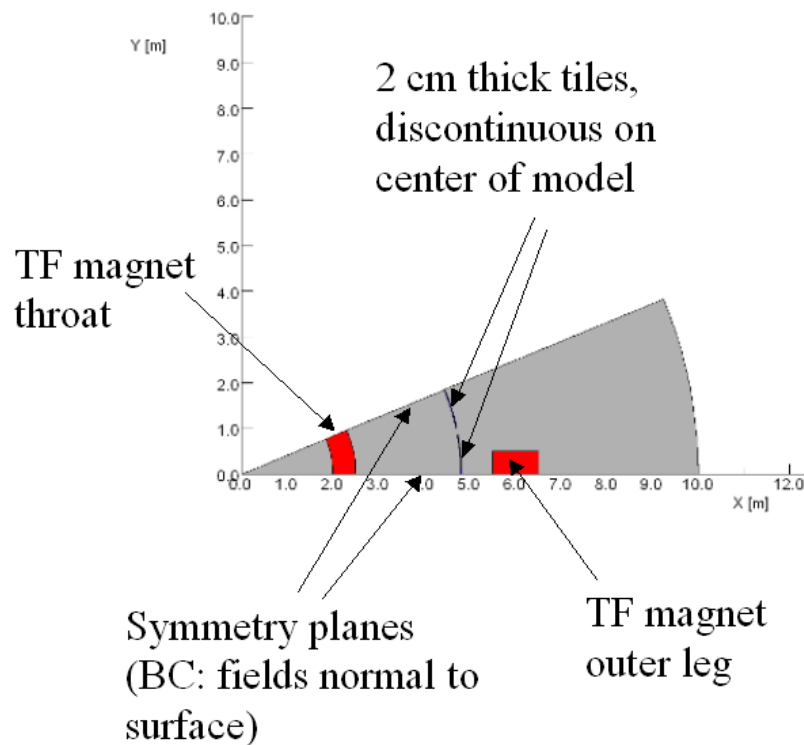


Figure 1. Schematic of geometry used to calculate the effect of multiple HTS monoliths on the toroidal field ripple in tokamaks.

The throat of the magnet is assumed to be continuous, with discrete legs in the outboard side. The symmetry of the problem was used to decrease the size of the required mesh. The planes with boundary conditions of normal magnetic fields are shown. It is assumed that the model is 2D, with coils extending in the direction out of the plane. Thus, the model is applicable to the midplane region of tokamaks.

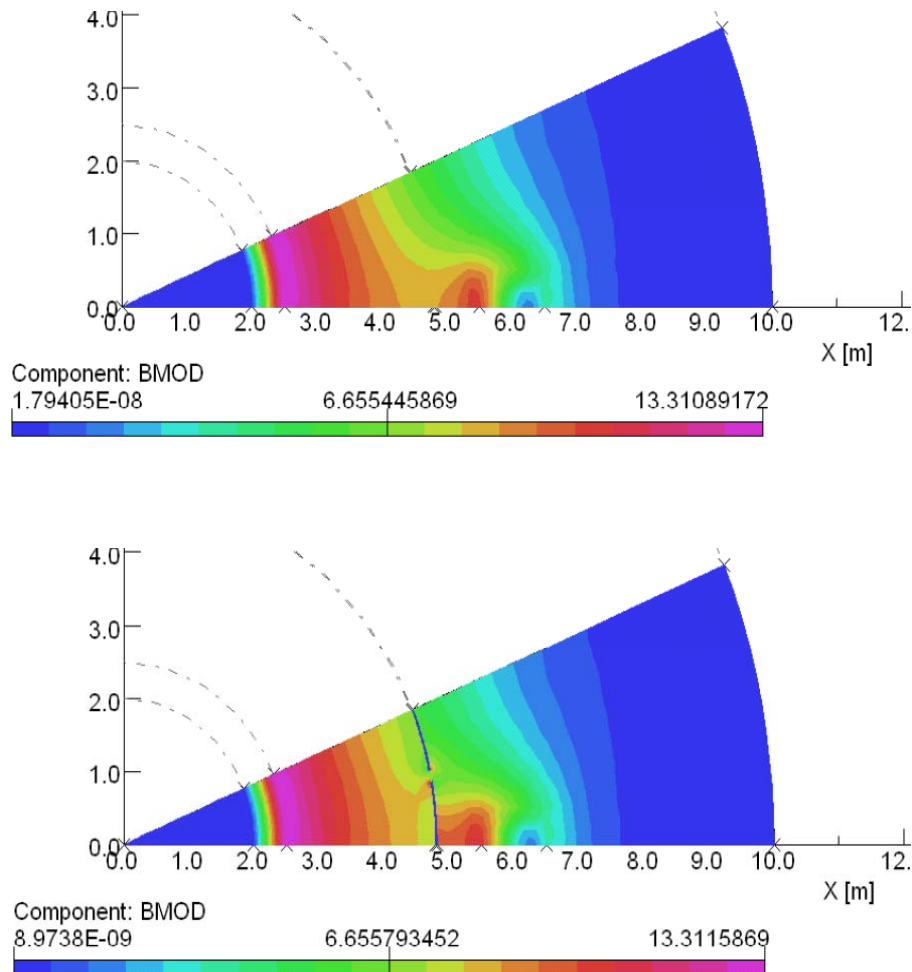


Figure 2. (a) Contours of constant magnetic field for the tokamak case with 8 coils and no HTS monoliths (base case)' (b) Same as (a) but with the presence of 16 HTS monoliths.

A. *Single layer of monoliths with 16 azimuthal monoliths*

The problem is solved using VectorFields Opera-2D software. The problem is solved with multiple adaptations of the grid until 0.1% accuracy of the solution is achieved.

Contours of constant magnetic field are shown in Fig. 2. Fig. 2(a) shows the results for no monoliths, while Fig. 2(b) shows the results for one layer with large tiles. Fig. 2(b) has 16 monoliths, with the centerline of one of the monoliths corresponding to the shadow of the TF coils. There is a substantial perturbation of the field around the region of the tiles, and also show is the effect of the gap. As mentioned before, the field tends to “squeeze out” between the monoliths.

The effect of smaller tiles, and multiple layers, will be described in the next section.

B. *Multiple layers*

Multiple layers of smaller monoliths is discussed in this section. There are 8 tiles in-between TF coils, or 64 tiles around the device. For the geometry chosen for the example, the monoliths are about 30 cm in width. In all cases, the thickness of the monoliths is assumed to be 0.02 m (2 cm).

The first layer of monoliths occurs at 4.8 m, and each subsequent layer is placed at 5 cm intervals, that is, the separation between layers is 0.03 m (3 cm). The gap between the tiles has been varied from about 0.01 m (1 cm) to about 0.04 m (4 cm).

Fig. 3 shows the resulting field profiles for the cases of 1 and 3 layers of 0.3 m monoliths. It is interesting to note the dark regions of high intensity magnetic field in between some of the tiles. The field is not prevented from penetrating through between tiles by the presence of monoliths downstream, but instead the field is guided in-between the tiles in a stair-case-like pattern. However, it is clear that the magnetic field ripple has been decreased, as the contours of constant magnetic field look more axisymmetric.

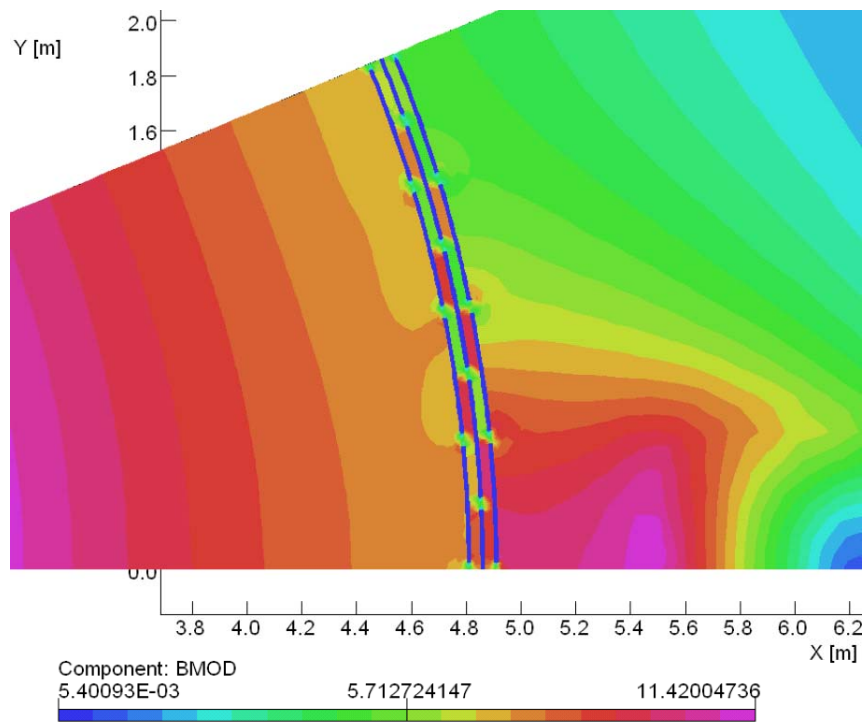
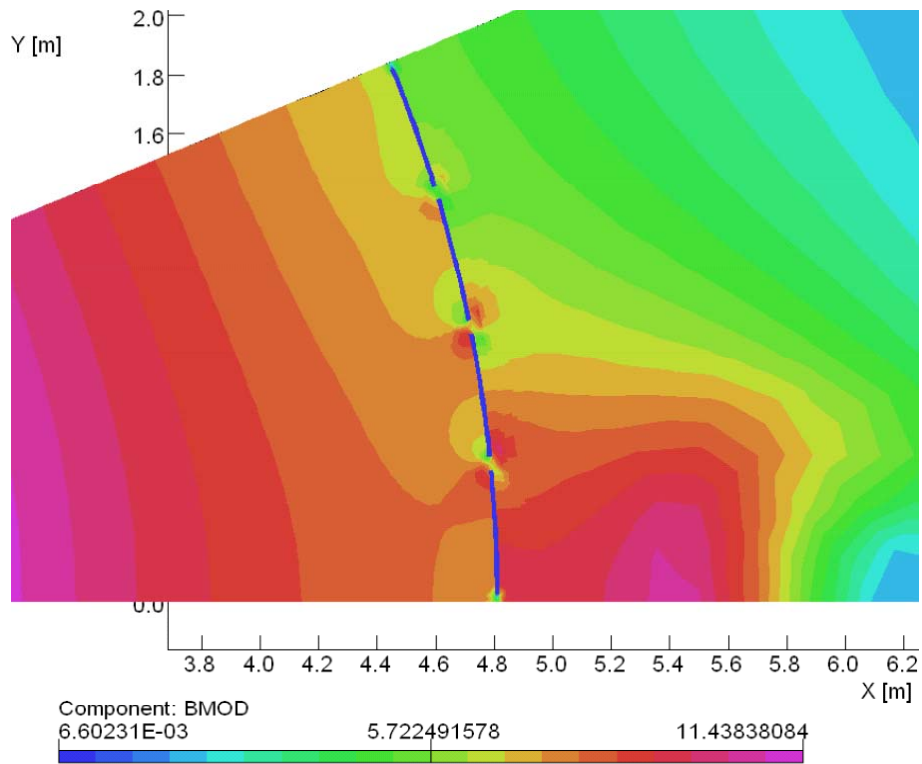


Figure 4. Contours of constant magnetic field. (a) for the case of a single layer of 0.3 m monoliths (b) for the case of 3 layers of monoliths with 3 cm between layers.

Fig. 5 shows the contours of constant magnetic field in the case of 5 layers of staggered tiles. The stair case geometry can be seen clearly in this case. The field “squeezes” out through the gaps in between layers.

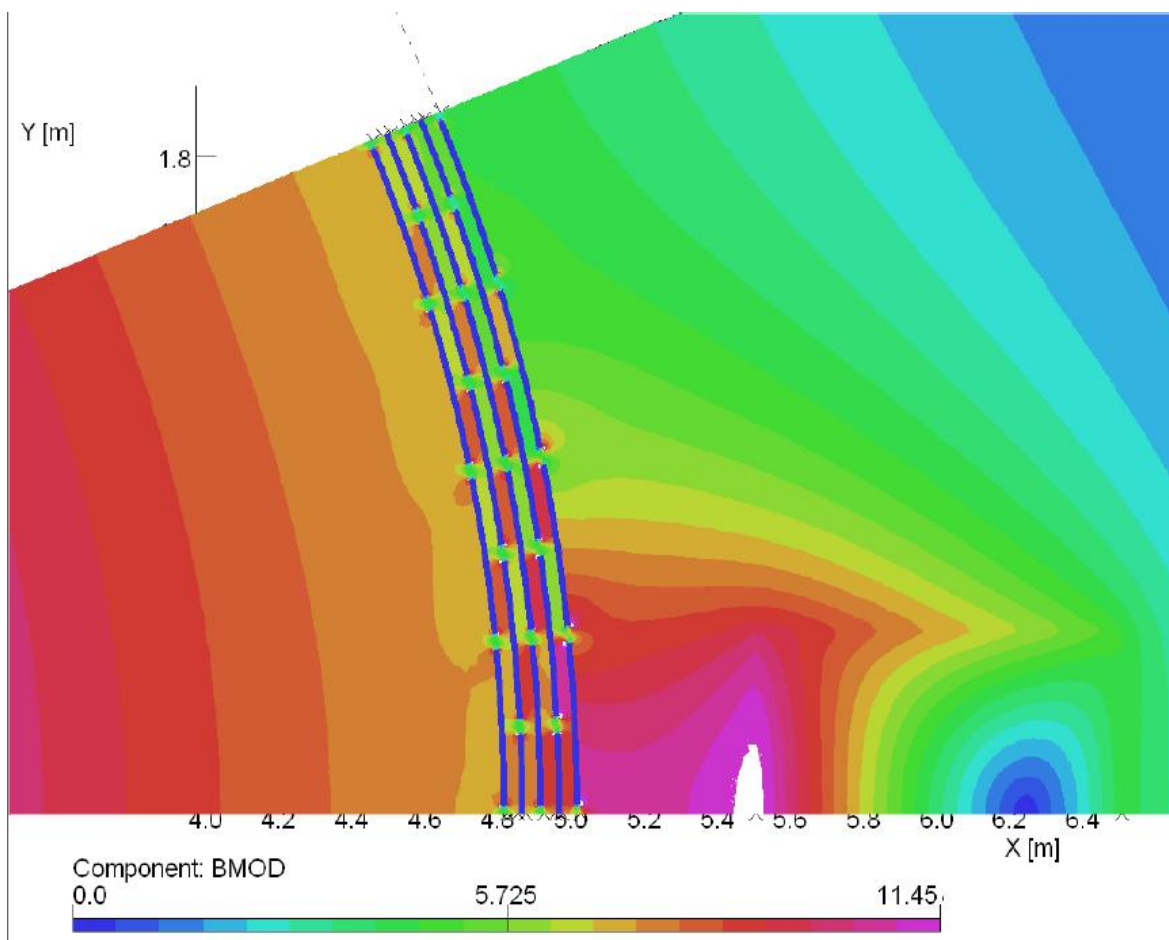


Figure 5. Contours of constant magnetic field for the case of 5 layers of monoliths with 3 cm between layers.

The magnetic field on the monolith surface, and the associated current density on the surface are discussed now. The case with 3 layers, shown in Fig. 4(b) will be used.

The magnetic field on the surface on the monoliths is shown in Figure 6. Shown in Fig. 6 is half-distance between coils, using the symmetry properties of the model. The field is shown from 0 degrees to 22.5 degrees, the point half-way between coils.

The field along the innermost and outermost surfaces (those with the small major radius and large major radius) of the monoliths are shown. Fig. 6 shows the fields on the first and the second row of tiles, as a function of the toroidal angle, which goes from the location under one toroidal field coil to the midplane between toroidal field coils (that is, $1/16$ of the torus, as in previous figures).

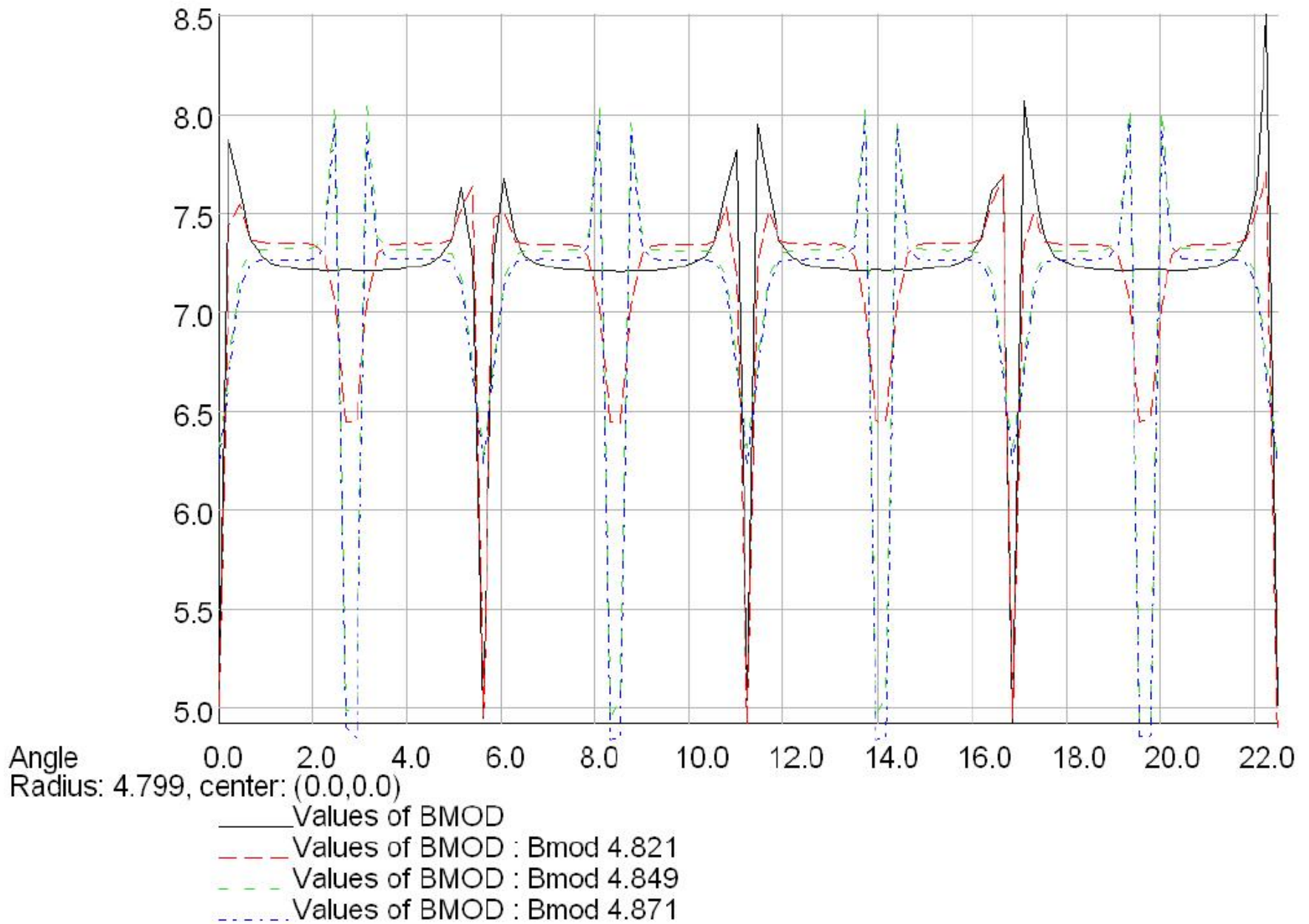


Figure 7. Magnetifc field at different radii as a function of the toroidal angle

The location of the fields are 1 mm from the surface of the tiles, thus for the first row of tiles, the field is shown at 4.799 and 4.821 m, since the tile goes from 4.8 to 4.82 m (0.02 m thick).

The fields are relatively constant on the middle of the monoliths, unless one of the sides is facing a gap in monoliths of the adjacent row. Thus, the first surface of the monoliths (at 4.799 m), which does not face an adjacent row of monoliths, shows large field perturbations only near the gaps in between monoliths. In this region there is a strong perturbation, with field increasing up to the edge, and then decreasing suddenly. The reason for the field decrease in the gaps between monoliths has to do with the diamagnetic field characteristics of the monoliths. The monoliths exclude all fields, including the main toroidal field, from the region of the monoliths (this can be seen clearly in the contours of constant magnetic field shown in Fig. 4b and 5.). Thus, in the shadow between the tiles, the field is much smaller and decreases the magnitude of the field in the neighboring regions at slightly larger or smaller radius than the monolith surfaces. This behavior occurs for all gaps between monoliths, in all layers. All of them show a decrease in the magnetic field magnitude in the region adjacent to a gap between monoliths.

It appears that the magnetic field is actually increasing radially (comparing magnetic fields at 4.799 and 4.821 m), and the field over the flat region of the monoliths are larger. However, when the magnetic fields are averaged along the toroidal direction, including the fields next to the gap regions, the average magnetic field at 4.799 is higher than that at 4.821 m.

The magnetic field along the second surface, at 4.821 m (right outside the surface of the first row of monoliths that faces away from the plasma) is more complicated than at 4.799 m. The field experiences a bump in the middle section due to the gap between the monoliths of the second row of monoliths. What is interesting is that the gap between monoliths in the adjacent layer of monoliths affects the field distribution in the middle of the monolith facing the gap.

The bump in the magnetic field has the same shape for all the gap. As the gap is approached, the magnetic field first increases, and then suddenly decreases in the region

immediately adjacent to the gap. The high value of the magnetic field on the edges of the monoliths implies substantially higher currents in this region. This issue will be discussed in the next section.

C. Currents in monoliths

The results showing the calculated current density (surface current density K , as described above) are discussed in this section.

The surface current density for the case with 3 layers is shown in Fig. 7. The current is shown for the first monolith (closest to the x-axis), as a function of the toroidal angle (between 0.25 and 5.375 degrees, as a result of a 0.5 degree gap between tiles). The magnitude of the current density is shown, in MA/m², assuming that the current is flowing in 1 cm thick region. The thickness of the current carrying region is an assumption for the plotting, and the actual thickness of this layer will be addressed in a later section. The currents flow along the surface, and in this approximation the current flow in a plane perpendicular to the main axis of the tokamak. The current flows in the toroidal direction in the wide regions of the monoliths, and the radial direction in the region of the monoliths next to the gaps. The current in between the gaps is not shown in Fig. 7.

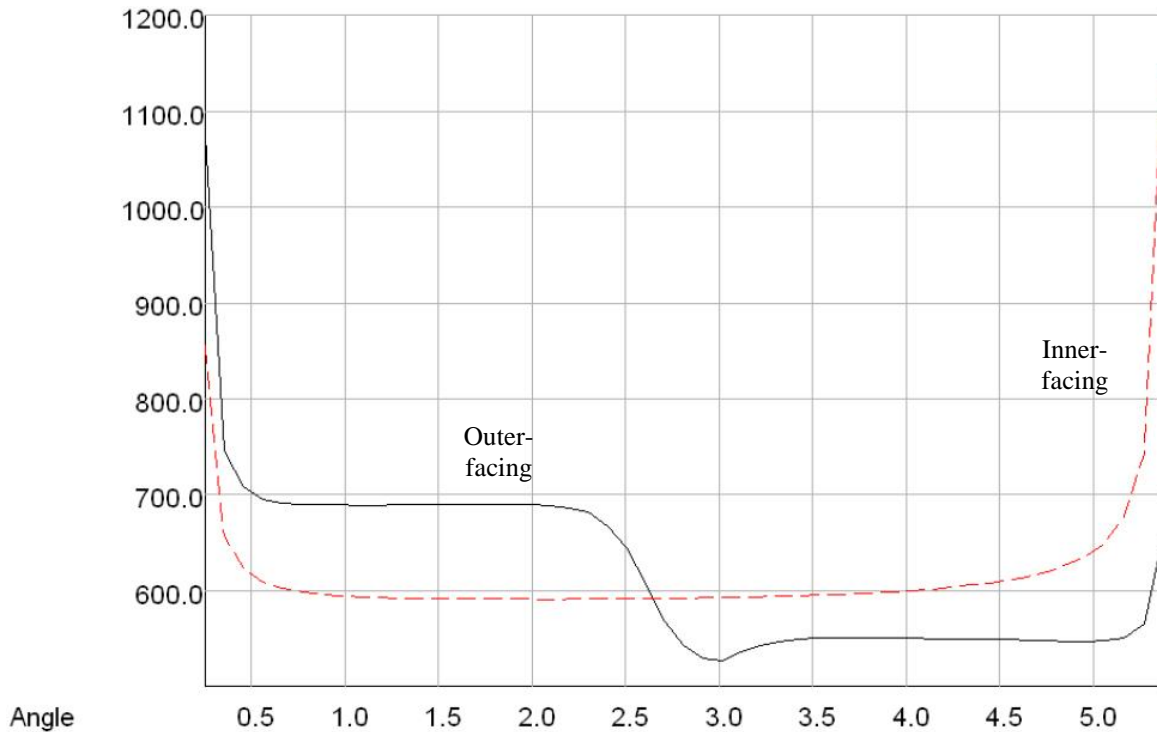


Figure 7. Current density (in MA/m²) flowing in the monolith under the toroidal field coil, for the first layer of monoliths (closest to the plasma), assuming that the current is flowing in a region of thickness of 0.01 m (1 cm).

The surface current on the first monolith on the first layer closest to the plasma (at 4.8) is relatively simple. It is flat in the middle, with large bumps on the sides, as the current work hard to prevent the presence of magnetic field on the edges of the monoliths.

On the other hand, the surface away from the plasma, at 4.82 m, has a interesting bump in the middle. This bump is due to field squeezing out in-between the gap of the monolith layer at 4.85, which is approximately at 2.5 degrees.

The current on the middle of the monolith only serves the purpose of preventing the toroidal field from penetrating into the monolith. However, it does little to reduce the toroidal ripple, or to shape the magnetic field.

The effect on the other tiles of the first layer of the monoliths is shown in Fig. 8. The behavior of the other monoliths is similar to that of the one discussed in Fig. 7. The side

facing the plasma, which does not face an adjacent layer of monoliths, shows a relatively flat magnetic field. The back side, which faces the second row, has the discontinuity at the middle, corresponding to the gap in the adjacent layer.

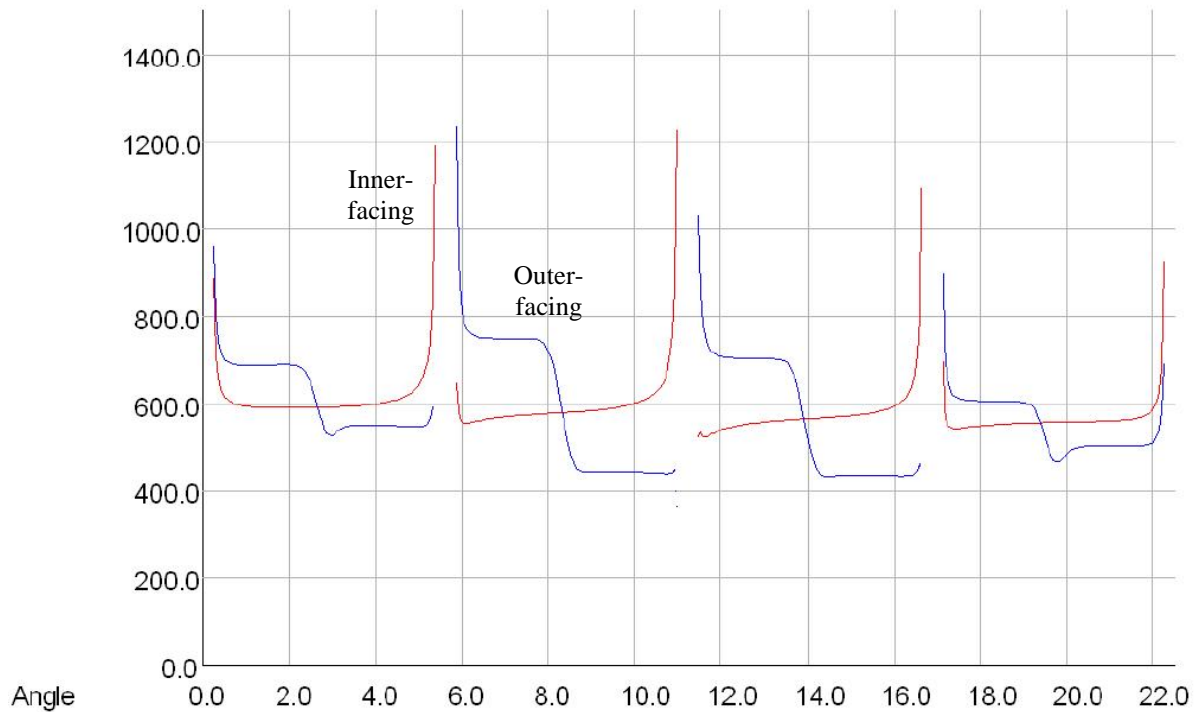


Figure 8. Same as Fig. 7 for the first layer of monoliths, assuming that the current is flowing in a region of thickness of 0.01 m (1 cm).

Figure 9 shows the current density on both sides of the second layer of monoliths. In this case, there are discontinuities on both sides of the monoliths, in the middle section, as both sides are facing against adjacent layers. Note that for the layer close to 0 and close to 22.5, the currents on BOTH sides of the monoliths are very similar. Although the currents are not exactly the same on both sides for the other monoliths, the reason is due to the fact that the magnetic field squeezes in-between tiles, and as the surface current and the field have a linear relationship, as the field changes, so does the current. But the modification of the field occurs due to the currents in the edges.

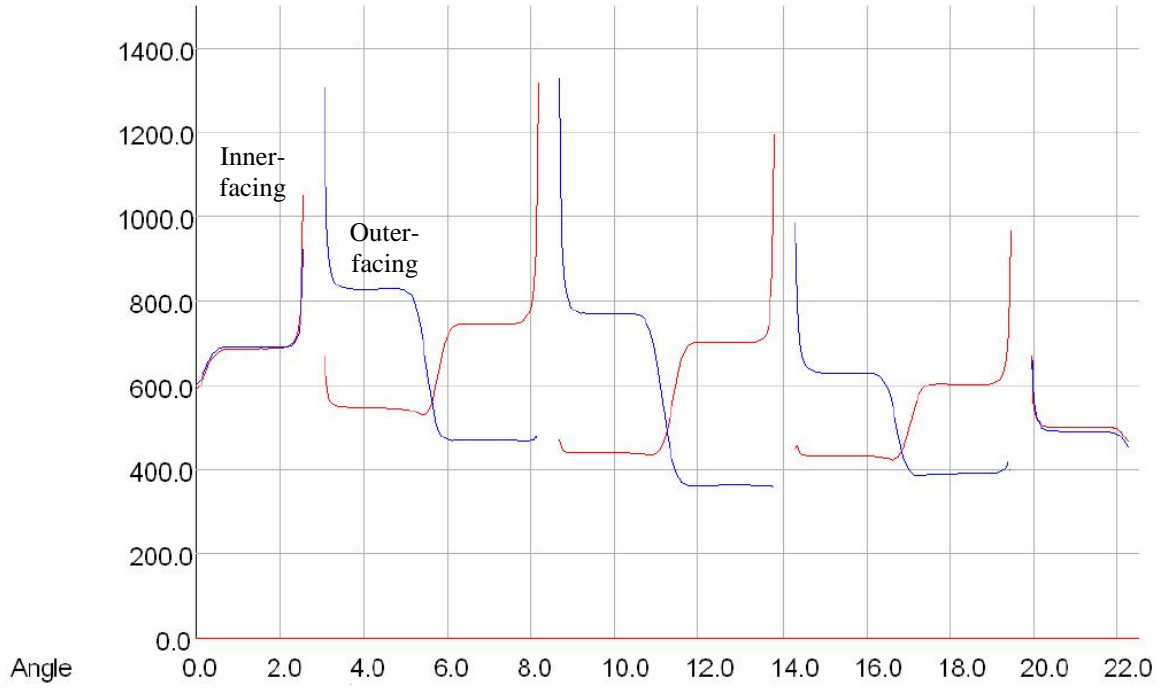


Figure 9. Same as Fig. 8 for the second layer of monoliths.

D. Decreased gaps between monoliths

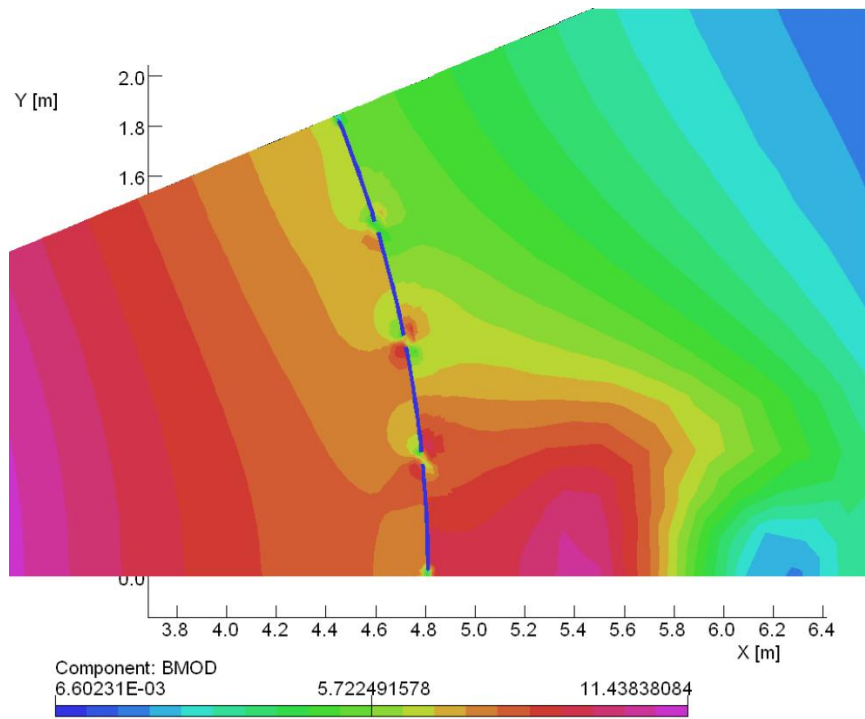
It is of interest to determine the effect of decreasing the size of the gap between monoliths in each layer. Since there is a substantial effect due to the presence of the gaps, the sensitivity to variation in the gap size was investigated. The work in the previous sections, as described, was for a gap of 0.5 degrees in-between tiles, corresponding to about 4 cm for the geometry described above.

In this section, we discuss the effects of a 0.1 degree gaps size, with is about just under 0.01 m (1 cm).

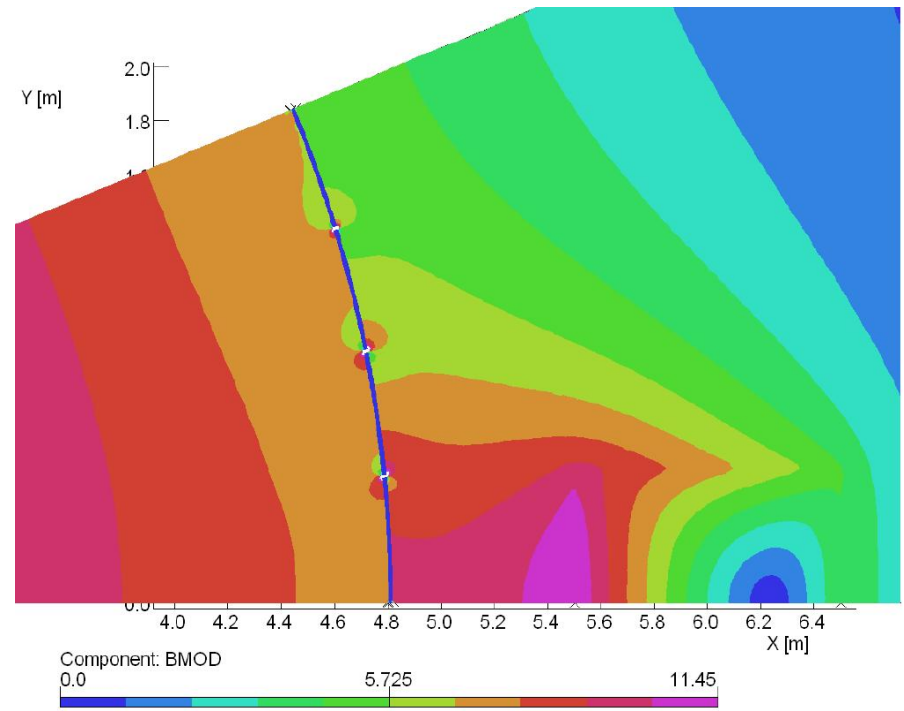
The contours of constant magnetic field for the case of a single layer of monoliths is shown in Fig. 10.

Clearly, there is still a lot of field perturbation by the presence of gaps between monoliths. The field contours, away from the location of the monoliths, look similar in both cases (see the contours around $R = 4$ m, with similar characteristics). The field profile, on the other hand, is substantially different close to the monoliths. The magnetic fields are substantially higher.

It should be noted that because of the finite current density and the fact that the current peaks in the region right next to the gaps in between monoliths, the effective gap is determined by both the physical gap and the thickness of the current carrying layer in the edge. As will be seen later, a 4 cm is appropriate.

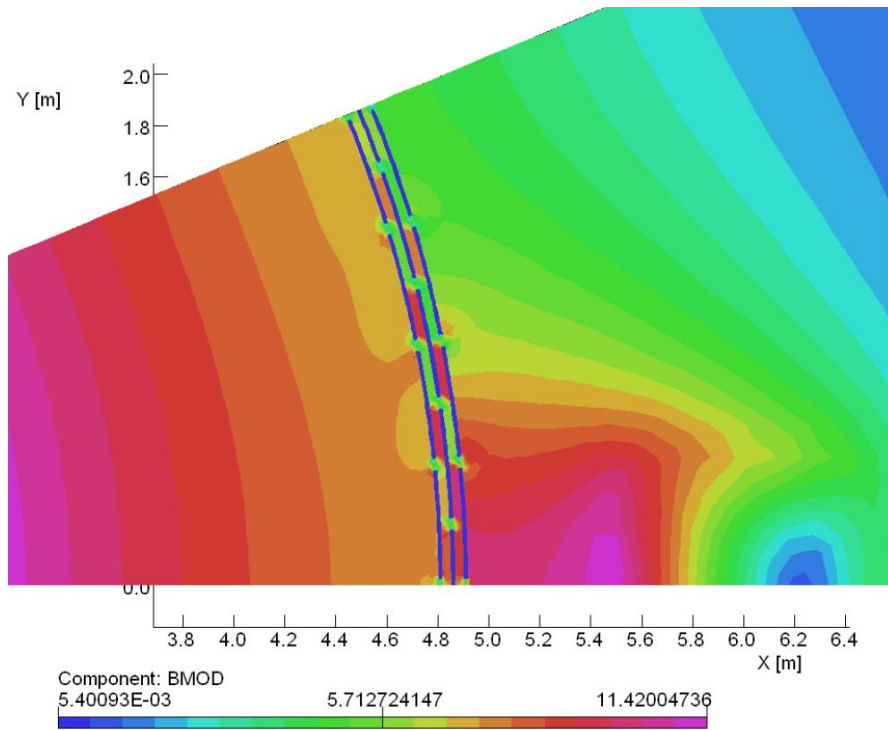


(a)

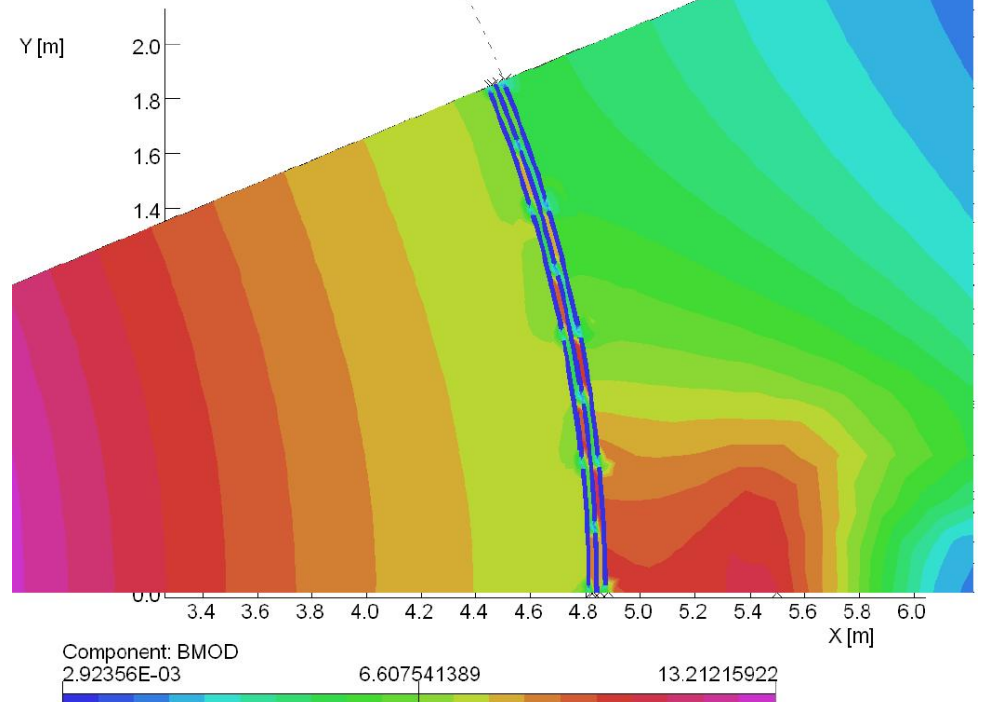


(b)

Figure 10. Contours of constant magnetic field for the case of 1 single layer of monoliths, for a gap between monoliths of (a) 0.5 degrees; and (b) 0.1 degrees.



(a)



(b)

Figure 11. Contours of constant magnetic field for the case of three layers of monoliths, for a gap between the monoliths of (a) 0.03 m and (b) 0.01 m.

E. Decreased radial gaps between adjacent layers of monoliths

In this section, we discuss the effects of decreasing the gap between layers. In the work described above, the period for the monoliths layers is 0.05 m (5 cm). Since the monoliths are 0.02 m thick, the distance between layers is 0.03 cm. The effect of decreasing the gap between layers to 0.01 m (1 cm) is discussed next.

The case considered is the same as shown in Fig. 4(b), with three layers of monoliths. The results are shown in Fig. 11 (a) and 11(b). Fig.11(b) is a replot of Fig. 4(b), replotted to make the comparison easier between the two cases.

F. Variation of the radial location of the monoliths

The case of tilting the monoliths with respect to the magnetic field is discussed in this section. The issue is that instead of placing the monoliths such that their main surfaces are parallel to the magnetic field, if they are tilted with respect to the desired fields, the squeezing out the magnetic field in between tiles can be decreased.

The geometry that has been chosen to illustrate the concept is shown in Fig. 12 (a), (b) and (c). A center of the circular pattern is chosen not to coincide with the center of the TF coils, but instead is moved by 20 cm . Thus, while the location of the monoliths under the TF coil (at a toroidal angle of 0 degrees) remains constant, at larger toroidal angles the major radius of the monoliths decreases with increasing toroidal angle.

In Figure 12(a) the circular path at 5 m is shown to indicate how the major radius of the monoliths changes with toroidal angle. Comparing 12(a) with 10(b) indicates that the solutions has indeed decreased the ripple in the region at the location in-between toroidal fields. However, the peak field at the edges of the monoliths, as shown in Figure 12(b) has increased, as the magnitude of the field that needs to be excluded from the monoliths increases (because of the orientation of the monoliths with respect to the toroidal field, with the monoliths “intercepting” a larger magnetic flux).

Figure 12(c) shows the magnetic field along a radius of 4 m. The ripple will be compared with the ripple from the other configurations in the next section.

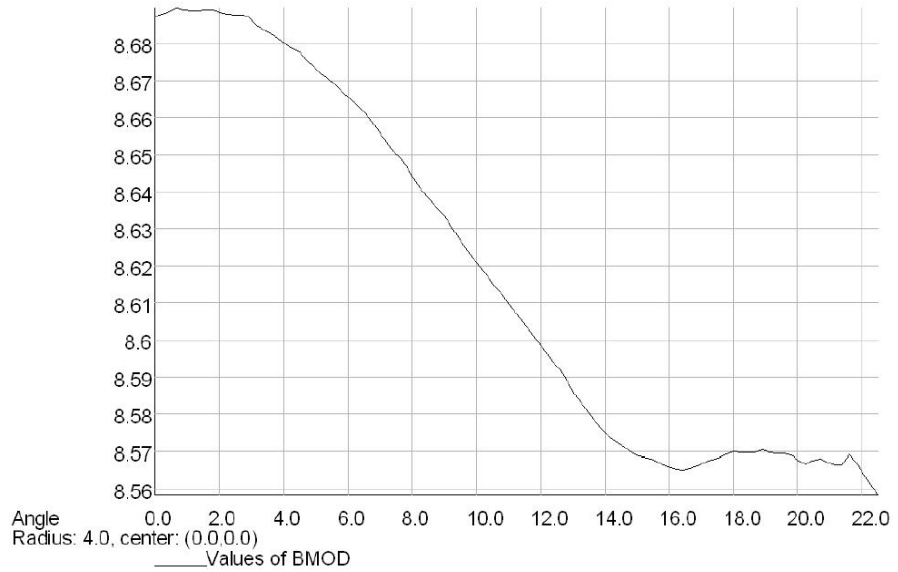
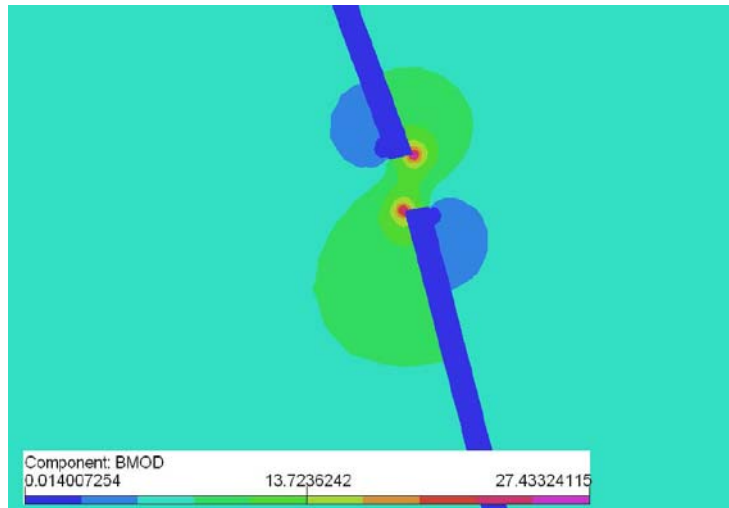
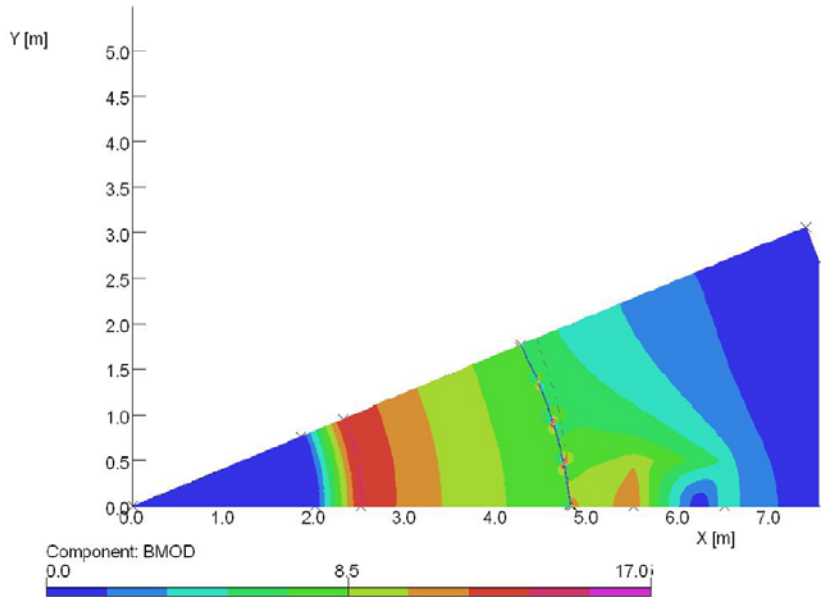
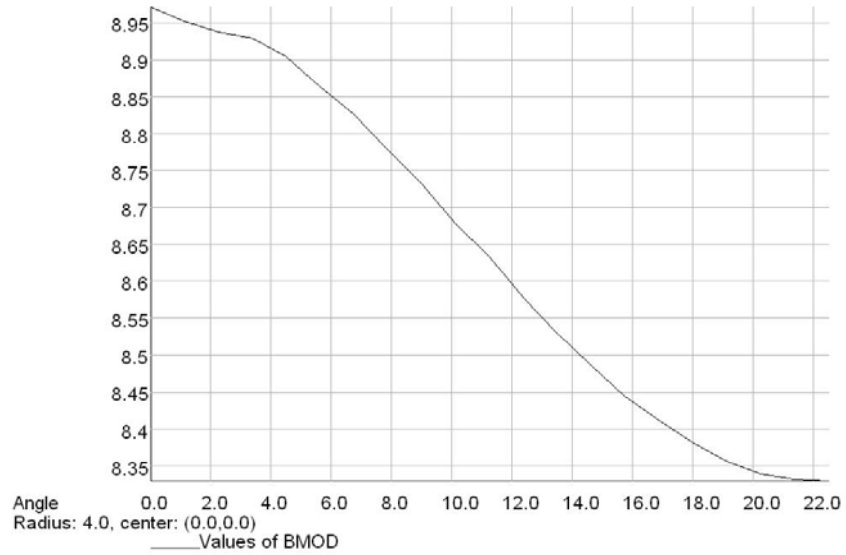


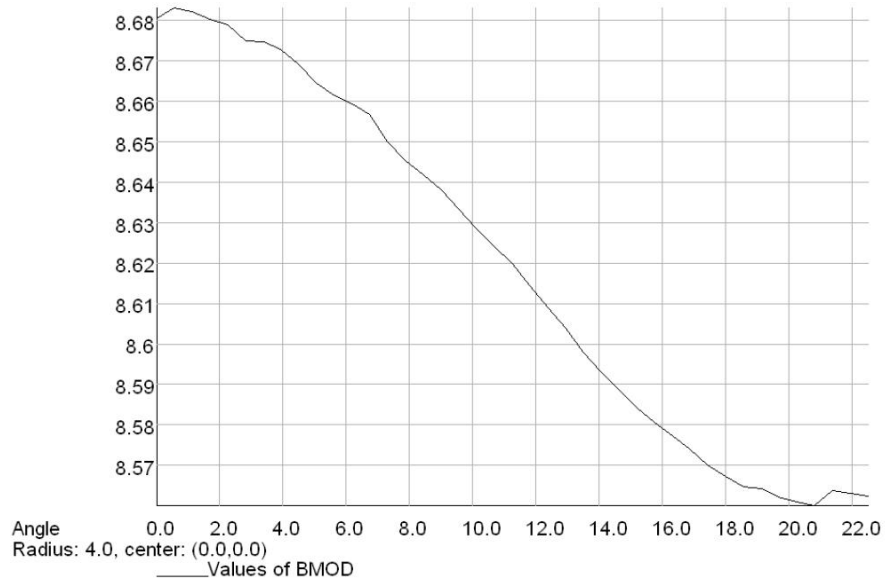
Figure 12. Contours of constant magnetic field as a function of the toroidal angle for a layer of monoliths that is tilted with respect to the direction of the axisymmetric toroidal field.

G. Magnetic field ripple

Fig. 13 shows the magnetic field along an arc at 4 m in the toroidal direction. Shown in Fig. 13 is half-distance between coils, using the symmetry properties of the model. The field is shown from 0 degrees to 22.5 degrees, the point half-way between coils. Two conditions are shown, one with no monoliths (shown in Figure 13(a) , and then with three layers of monoliths, shown in Figure 13(b)



(a)



(bb)

Figure 13. Magnetic field magnitude as a function of the toroidal angle for (a) the case without monoliths and (b) for the case with 3 monoliths with a 0.5 degree gap between monoliths and 3 cm between layers of monoliths.

As can be seen from Fig. 13, the field ripple is close to sinusoidal in both cases, with the fundamental dominating. There are no higher harmonics visible in the field, showing that the field from the individual monoliths has “washed” out.

The corresponding values of peak-to-peak ripples is shown in Fig. 14, as a function of the number of layers. The field ripple is about 7% in the absence of correction by the monoliths, and decreases exponentially with increasing number of layers. The exponent is about 0.5. Between 4 and 5 layers are required in order to bring the ripple down to below 1%.

Also shown in Fig. 14 is the ripple for the case with decreased gap between monoliths. In the results up to now the gap between monoliths is 0.5 degrees, corresponding to about 0.04 m between tiles. The point indicated with 0.1 degrees between monoliths in Fig. 5 corresponds to about 0.008 m between monoliths.

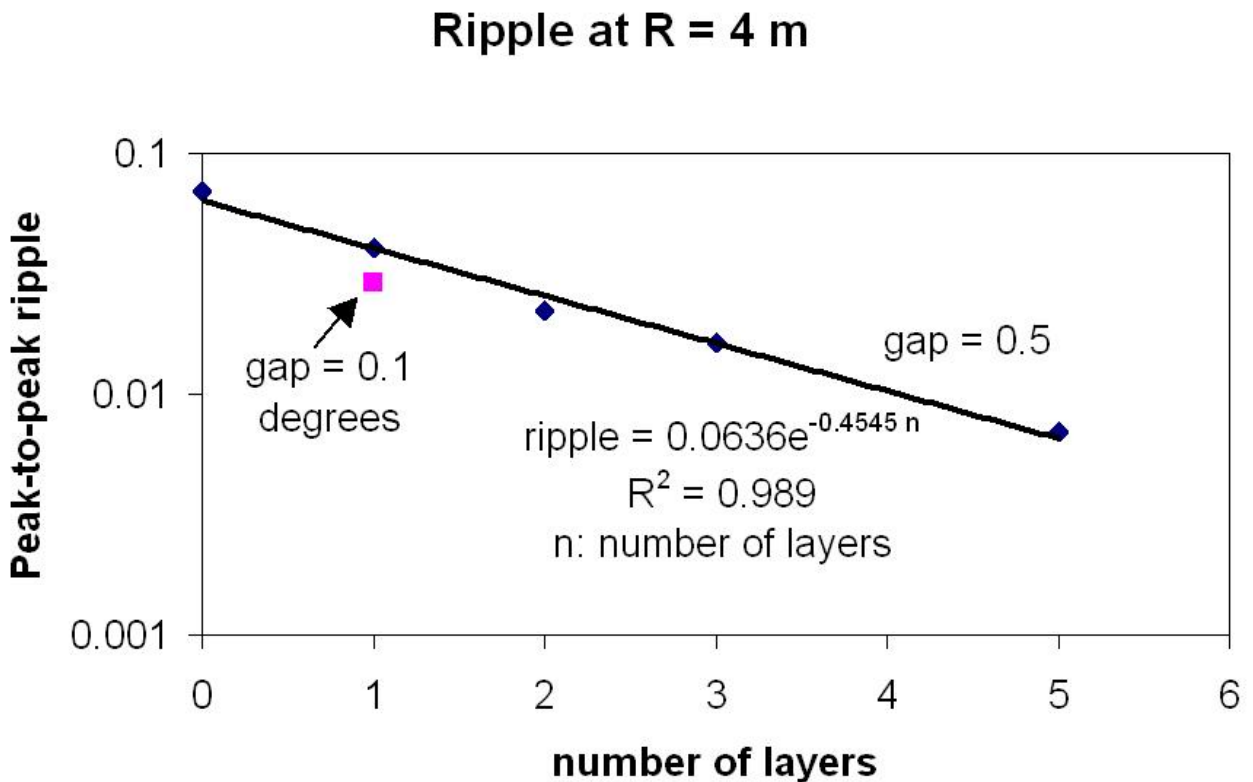


Figure 14. Peak-to-peak ripple at 4 m as a function of the number of layers, for two cases of gaps between monoliths.

Discussion

Although the results are for infinitely long monoliths, the results are expected to be relevant even in the case of limited extent of the tiles in the poloidal direction.

The thickness of the current carrying layer can be determined from these results. It is on the order of 1 cm, so that assumption of perfectly diamagnetic monoliths, although not exact, does provide a good insight into the performance of the monoliths for shaping fields in toroidal geometries.

The current density in YBCO material (high quality, epitaxially grown by SuperPower Inc) is shown in Figure 15 as a function of the angle orientation between the planes of the crystal and the magnetic field.

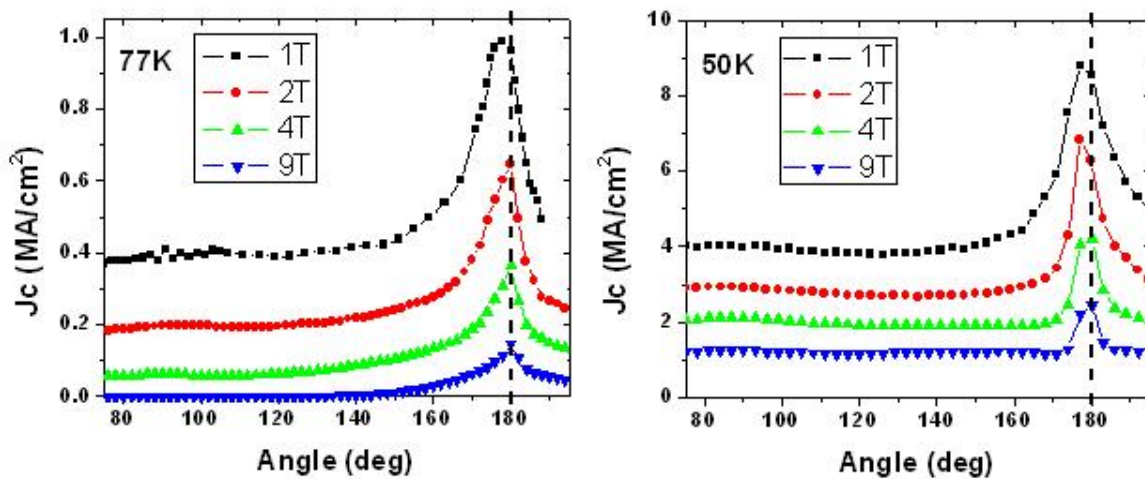


Figure 15. Critical current in the superconductor as a function of the angle between the planes of the crystal and the applied magnetic field, at 77 K and at 50 K. Epitaxial YBCO (private communication, SuperPower Inc).

At temperatures of 77 K, the maximum useful magnetic field is around 4 T. However, at 50 K, even with 9 T applied in the bad direction (that is, with the magnetic field perpendicular to the planes in the crystal), the current density is about 1 MA/cm².

In the above section, it was described that with a 1 cm thick current carrying layer, the required current density in the superconductor is about 1000 MA/m², or 0.1 MA/cm². Since the current density, even in the bad direction of the superconductor, at 9 T, is one order of magnitude higher. This means that the layer of superconductor is about 0.1 cm, or 1 mm.

The superconductor material in Figure 15 is highly optimized, epitaxial, with thin dimensions. Bulk materials of intermediate quality have been made. Figure 16 shows the field profile, on the surface of a YBCO monolith, at 29 K, the highest field trapped in this material [Tomita]. From this data it is possible to derive the approximate current density

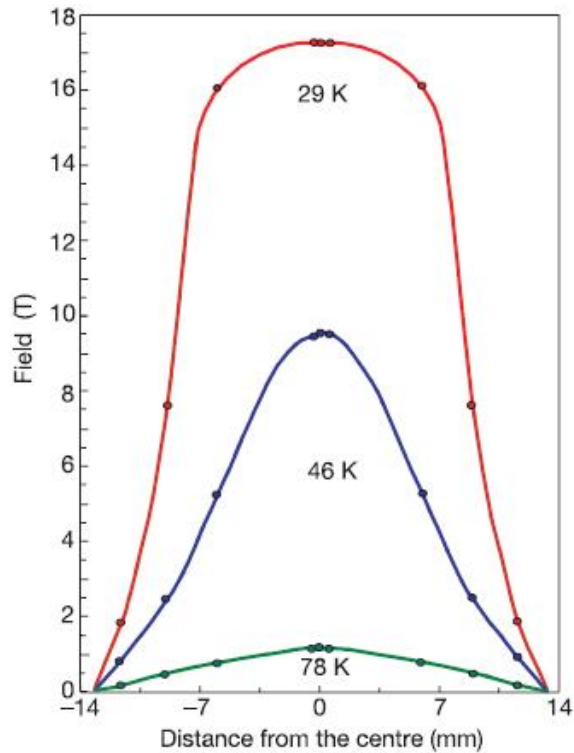


Figure 5 The effect of temperature on trapped-field distribution. The field was trapped between two 26.5-mm-diameter YBCO disks with carbon fibre wrapping, resin impregnation and embedded Al. Data are shown for 29 K, 46 K and 78 K. It is evident that the trapped field is saturated at higher temperatures, but that the field is far below saturation at 29 K, showing that much higher fields could be trapped.

Figure 16. The effect of temperature on trapped-field distribution between two 26.5-mm-diameter YBCO disks Data are shown for 29 K, 46 K and 78 K. [from Tomita]

It is evident that the trapped field is saturated at higher temperatures, but that the field is far below saturation at 29 K, showing that much higher fields could be trapped.

The results shown in Figure 16 were obtained by reinforcing bulk YBCO samples with carbon fiber wrappings, resin impregnation (both for strength) and aluminum (for increased thermal conductivity). Fig. 17 shows a SEM pictures, as well as the final product.

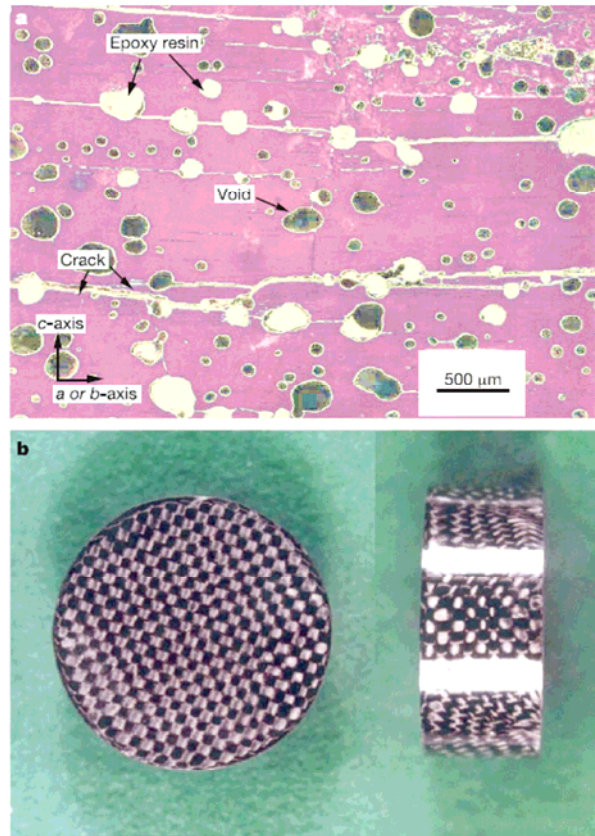


Figure 17. SEM picture and final product disks.[from Tomita]

The calculated current density in the pucks is on the order of $2 \cdot 10^9 \text{ A/m}^2$ at 17 T and 29 K. This number is consistent with those of the epitaxial deposited materials, maybe a little lower.

With these values of current densities, it is clear that large cross sections of the HTS materials were not carrying any current. They need to be made much thinner, on the order of a few millimeters. It is difficult to make this thin YBCO materials, as the surface of the bulk monoliths usually have poor quality. But it is possible to produce thin YBCO monoliths, with some development, according to some of the manufacturers [Werfel].

Thinner superconductors will prevent the use of material that does not contribute much to correct the field, but the contribution to correcting the field is also reduced by going thinner.

As mentioned above, the current through the middle of the monoliths does little to correct the field, most of the field correction is carried out by currents flowing in the edges of the monoliths. That is, instead of disks, the same performance can be obtained with thin rings, substantially decreasing the required material.

At the present time, the cost of the monoliths is close to the cost of the materials and the electricity required for their manufacturing. The present costs of these materials are estimated to be about 15000 €/m², or about 15 €/cm². [Werfel, Hobl]

An alternative to making HTS monolith disks is to make HTS rings of the material. Much less material is required, resulting in savings in costs, cryogenic thermal loads (lower radiation, both thermal and nuclear). Future studies should investigate the use of monolithic rings, rather than disks. The charging studies described in the

Finally, it is also possible to make the rings from wound tapes. The advantage of these tapes is that they can be driven, and do not have to be subject to field creep into the materials (which results in a decay of the field and in heating of the monoliths). The decrease of the field is of great concern when the monoliths are being used for modification of the steady state fields.

IV. STELLARATOR GEOMETRY

The complex geometry of the stellarator is presently being investigated using the same model. Figure 18 shows the model built to investigate the performance of the bulk monoliths.

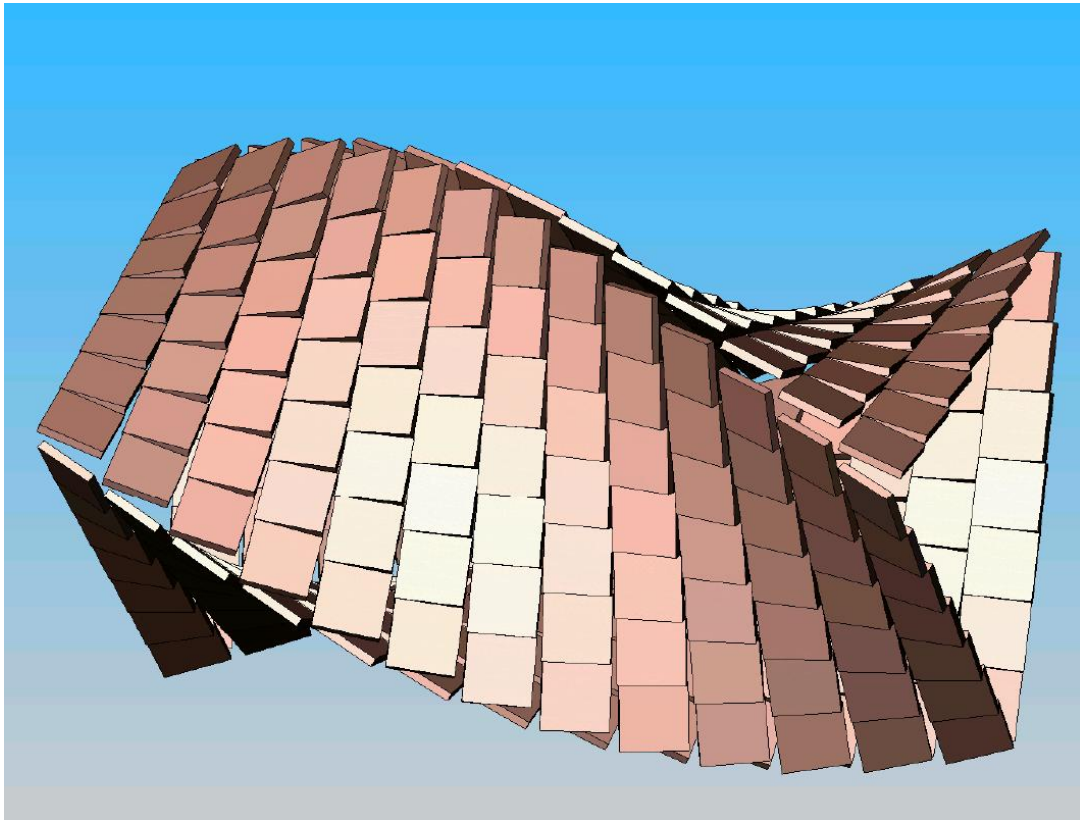


Fig. 18 Tiles distributed along a helical surface as a model for the stellarator.

This program ended before we were able to complete the work with the monoliths. However, it is possible to make some conclusions about the application of HTS bulk to stellarator windings.

V. CHARGING AND FIELD CREEP

In this section, we report on measurements performed on HTS material.

The material used in this research was BSCCO 2212, provided from Hoechst AG in Frankfurth, Germany. The material was processed by the melt cast method, providing adequate orientation of the grains. The tests were done as part of a program to determine the applicability of this material for NMR inserts [Bromberg], but are relevant for the present discussions and not reported elsewhere.

The material was tested in a high field magnet. Good Superconducting properties were determined at high fields (20 T). However, the uniformity was not adequate. After discussion with the manufacturers, we determined that the material was prepared using a silver sheet that protruded into the superconductor, and therefore the material was not homogeneous. A separate material was acquired and tested, without the silver material. Under these conditions, the material was more uniform, but measurements indicated that the material was still not sufficiently homogeneous, producing field errors not present in the charging field.

An alternative approach was then attempted, using the monoliths, that included a silver contact at both ends, as a monolithic coil. The superconducting material was mechanically machined as a coil, and then tested. Although the principle was shown to work, the achieved current density in the tests was disappointingly low. As with the monoliths, the problem is associated with non-uniform quality of the material.

The material was prepared by Hoechst AG via the melt cast process. Oxides of Bi, Sr, Ca, and Cu, together with certain amount of SrO_4 as ad mixture are molten in a furnace operating at 1000 - 1200 C. The melt is then poured into a rotating mold, where the material solidifies. The process is sensitive to the speed of rotation and the rate of change of the temperature. A post-heating of the solidified melt to allow a slow and defined cooling to room temperature is essential for a crack-free piece. The result from this process is a heterogeneous material, with reduced oxygen content, but with the final shape. The annealing process is performed in an oxygen atmosphere at temperatures around 800°C, close to the material melting temperature. The rapid and complete transformation is favored by the formation of a

partial melt in the solid body. The material is thus transformed to the appropriate superconducting 2212 phase. The cast and annealed material has excellent machining characteristics. The material is surprisingly malleable, making it easy to cut, grind, or drill. Electrical contacts are achieved by placing folded silver sheets in the mold prior to casting the melt. Low electrical resistivity is obtained by interaction between the partial-melted and the silver during the annealing process.



Figure 1. High T_c tube tested. Shiny material is silver sheet applied during manufacturing process

The material, as sent by the manufacturer, is shown in Figure 1. The superconductor is the dark material in the inboard of the tube, which as mentioned above is BSCCO 2212. The external shiny material is silver, which was placed there for achieving quench protection/stability of the tubes, which were designed for current lead applications. Although

the silver results in good thermal transport from the cold temperature to about 77 K (the temperature of liquid nitrogen), its presence was necessary to provide an electrical shunt for the superconductor in case of the superconductor going normal. In the absence of the silver, the superconductor will overheat during a normal transition, and be destroyed.

Unknown to us at the beginning of the experimental program, the silver penetrates the superconductor material. The silver material through which the superconductor can be seen in the outer side of the cylinder has been punched in, and the piece penetrates into the superconductor. This is in order to provide a better electrical contact between the superconductor and the silver shunt. This penetration into the superconductor material does not affect the performance of the current lead, but affects the present application, where defined current paths are necessary for the monolith to reproduce closely the imposed external magnetic field. Therefore, after several attempts to produce high quality magnetic fields, we contacted the superconductor manufacturer, who provided us with material without the silver. They provided two tubes, one with 35 mm ID and a second one with 50 mm ID. The 50 mm ID material is shown in Figure 2. In this figure, a copper winding has been set around the superconducting tube, in order to determine charging characteristics. Individual charging characteristics of the 35 and 50 mm tubes have been performed, although in this report, we will describe mostly the results from the two tubes used simultaneously.

A. *Experimental assembly*

The design and construction of the setups that were tested in this program are described in this section.

In order to test the cylinders together, a probe was built to be tested in the presence of large magnetic fields. A schematic of the probe that was built is shown in Figure 3. Although it is shown for the case of two tubes, the arrangement is the same for the single tube. Axial Hall probes, calibrated by collaborators from the Leningrad Institute of Physics in Russia were used in the experiments. The advantage of using these probes was that they were expendable, and care for them, in particular during disassembly, was reduced. The probes were tested at a few points using known calibration of the magnets, prior to cooling the

superconducting tubes. The temperature of the tubes was determined by using a Au-Fe-Cr thermocouples. These thermocouples had been found to be very sensitive in the range of temperatures that were explored. The thermocouple used was carefully calibrated by the manufacturer. The thermocouple was located on the outer tube, and was thermally attached to bandage in the outer tube by epoxy, as shown in Figure 3.

We have used two methods of charging the tube: a) the magnetic field is applied, followed by cooling the tube to superconducting temperatures, and b) the tube is superconducting, but the applied magnetic field is varied to charge up the superconducting tube. For low temperature superconductors, the first method is always preferred. We have found out that for high temperature superconductors the second method is preferable, as will be described below.

The tubes were allowed to warm up with field trapped, without any applied background field. In this manner the critical self field (the field generated by the critical current at a given temperature) was determined.



Figure 2. Photograph of 50 mm tube, manufactured without the silver sheet

In order to provide support to the tubes when charged to full current and operating at the high fields, Be-Cu and Inconel was used as reinforcement. In the case of Be-Cu, the wire was wound in the outside of the tube, tightly around the superconductor. During cooling down, the coefficient of thermal contraction was such that the Be-Cu support ends up in tension, while the superconductor is under compression. Estimates on the compression stresses in the superconductor (with limited knowledge of the thermal contraction of the superconductor) indicated that the superconductor would be under the stress of about 70 MPa.

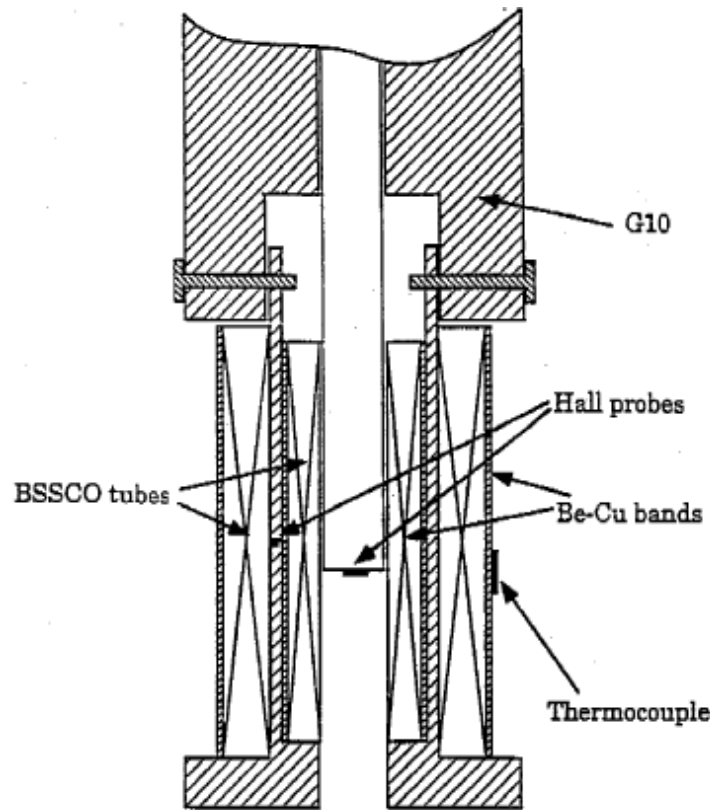


Figure 3. Schematic of the arrangement with two tubes, indicating location of tubes, support, thermal resistor (for temperature measurement) and axial Hall probes

The background magnetic field was generated in a magnet at the FSU's National High Magnetic Field Laboratory in Tallahassee, FL. This externally generated field was used both for producing the background field as well as charging the superconductor. We will present results from both the single and double tubes.



Figure 4. End view of assembly tested at 4 K with two tubes (50 mm and 35 mm).



Figure 5. Side view of assembly tested at 4 K with two tubes (50 mm and 35 mm).

Figures 4 and 5 show the end view and the side view of the arrangement with two superconducting tubes. The reinforcement (Be-Cu) is partially visible. The copper pieces that

extend to the end of the magnet are used for axial cooling of the tubes. This arrangement was made for testing that was to be performed at the later part of this program, with the use of a cryocooler. The charging mechanism described in the proposal (flux pumping) results in substantial dissipation in the superconductor (as the magnetic flux penetrate through the material, while it is in the normal or at least, flux-fluid state).

B. Magnetic field as a function of temperature

The magnetic field for a single tube (in this case, the 35 mm tube) is shown in Figure 2. The field at temperatures lower than about 10 K is not the maximum field, but the magnet is at its boundary with normal state (for conventional superconductors, in the current sharing state). At the value of the magnetic field in the figure, the current is the maximum current where the tube is in the superconducting state. As the temperature goes up, dissipation (quickly removed) results in a reduction of field.

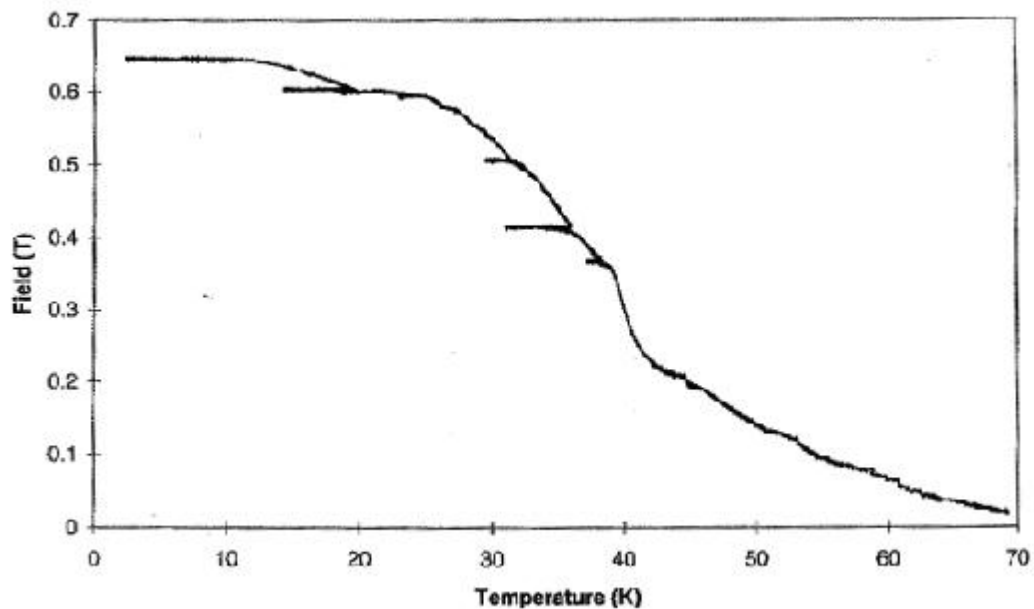


Figure 6. Magnetic field as a function of the temperature of the sample. Single 35 mm tube.

Figure 6 indicates that this superconductor is fairly good up to temperatures of about 25-30 K. At the higher temperatures, the current density is substantially degraded. The maximum field, per tube, at the lower temperatures, is about 1.2 T. The self field, as a function of the background applied field, is not a strong function of the background field at temperatures lower than about 10 K. At higher temperatures, the current density for current sharing state decrease with increasing field. BSCCO 2212 is not a great superconductor at temperatures greater than about 25-30 K, because of the lack of superconducting flux pinning at the higher temperatures. There is substantial commercial interest to develop, instead of BSCCO 2212, the much more difficult to produce BSCCO 2223, which has much better properties at higher temperatures, but that requires large efforts to obtain adequate texturing of the grains in the materials.

C. Magnetic Field Stability as Function of Temperature of Operation

For applications to NMR as well as to stellarator field shaping, field stability is very important. In this task, the stability of the field produced by the monolithic superconductors is explored.

The charging mechanism (flux pumping), requires that the material be at the normal state, or at least the flux melting state (current sharing), where the magnetic field can penetrate through the superconductor. Because of this requirement, after the charging state, the superconductor remains very close to this state. The field stability is therefore determined by the index of the superconductor, which relates the seen voltage to the current. The higher the index, the better the superconductor and the more stable it is after a transient.

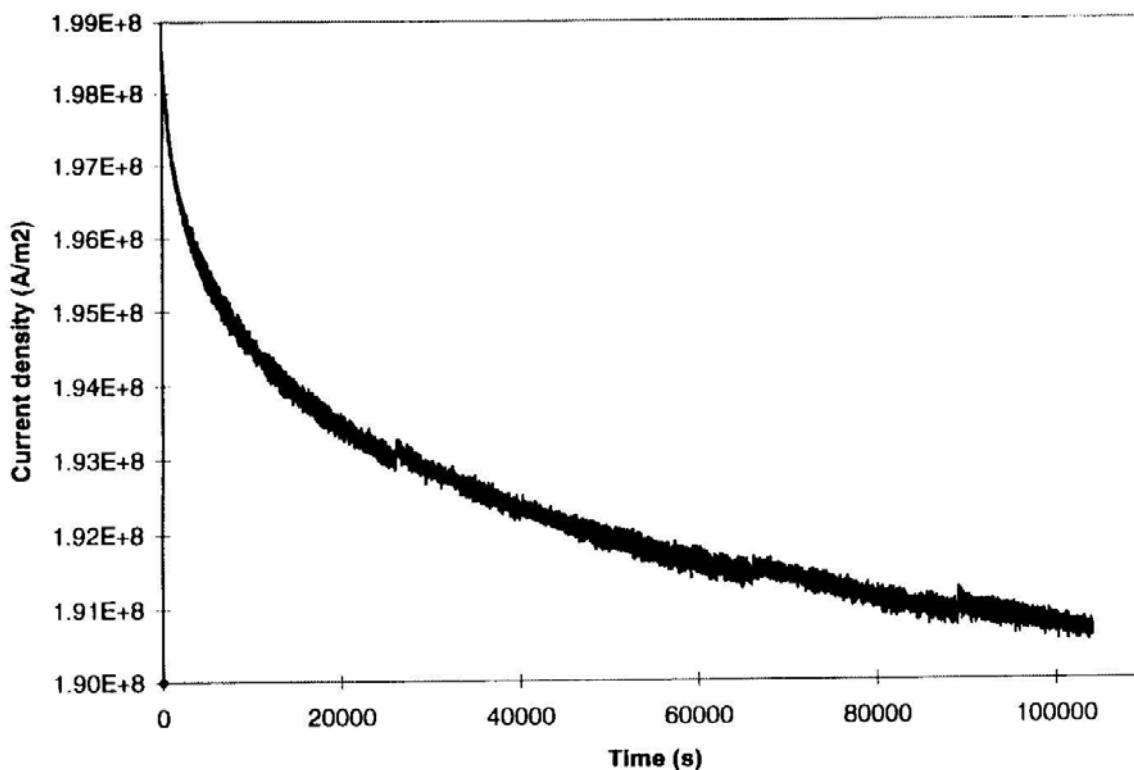


Figure 7. Current in the superconductor as a function of time, after end of charging state

As in typical magnetization measurements, the current density is not symmetric. The field profile in the tubes at a given value of applied field is different during ramp-up than during ramp-down. During ramp-down, the average field in the tubes is smaller than the field in the center of the tube, while during ramp-up the average field is larger than the central tube. At fields above 3 T the critical current in the reverse direction (for shielding) is approximately the same as the critical current in the positive direction (during ramp-down), due to the insensitivity of the critical current density on the magnetic field at these high fields.

After a flux meltdown (quench) the current does not disappear altogether, but retains a substantial fraction of the pre-quench current. The tube current after quench seems to be a constant fraction of the critical current. During the ramp-up at low fields, there are sporadic quenches. At the higher fields, the quenches become more regular. Also, the tube current after quench is larger in the case of ramp-up than in the case of ramp downs. It is not clear why the tubes retains any field after flux meltdown, but it must have to do with the high

critical temperature of the tubes. (So even if it quenches and heats up, it does not lose all its current carrying capability).

To explore the effect of ramp rate, lower ramping times were explored. Ramp rates of the background field of 0.05 T/s (5 minute ramp rate) to ramp rates of 0.25 T/s (1 minute ramp-down) were tested. The current density in the tubes prior to quench decreases, with the consequence that the quenches occur at smaller field intervals. It is interesting to note that the current in the magnet after the quench is larger in the case of the faster ramp rates. Even when quenching at the higher fields and at the fast ramp rates, some current remains in the tubes after the quench, i.e. the quenches are partial. The reason for the different behavior as a function of ramp rate is not understood at the present time.

On another set of experiments, the rate of change of the field at liquid helium temperature was recorded. The tube was charged by increasing the applied magnetic field and then very slowly decreasing the field. The resistive magnet was then turned off, and disconnected, i.e. the background field was zero. The generated field was due to the superconductor, which at the beginning of the test the tube was at critical or very near critical conditions.

The magnetic field in the tube was monitored. The liquid helium was periodically replenished. The duration of the test was limited, since we needed the setup for measuring other tubes. The time behavior of the current density in the magnet is shown in Figure 7. The decay of the field or current density during the test was about 0.5%, with most of the decay occurring shortly after charging the tube.

The time constant for the decay of the field, $\tau^{-1} = (1 / B) dB/dt$ is shown in Figure 8 as a function of time. The time constant for the decay of the current increases with time. The noise at the larger times increases due to the decrease in the decay rate with time, requiring larger averaging. However, a regression obtained with from this data shows a constant slope. A quadratic regression gives approximately

$$\tau \sim 98.6 t + 1.8 \cdot 10^5 \text{ seconds.}$$

The quadratic term is small, and the slope of the curve is approximately linear. By increasing the time for averaging the signal, the noise at the longer times can be substantially decreased. These results show clearly that the time increases with a constant slope. The consequence of this measurement is that the current (or self-field) decays at a relatively high rate soon after charging, but remain at constant field for a long time afterwards. The time constants at the end of the testing (about 1.5 days), is on the order of 10^7 s, i.e., several months. In this manner, it is possible to flux trap fields that are persistent. All that is needed is to charge them slightly below their critical self-field.

If a fit $V \sim I^n$ is used to describe the superconductor (where n is the index of the field), it can be determined using a best fit, that $n \sim 120$. These high values of the field have also been measured using other techniques.

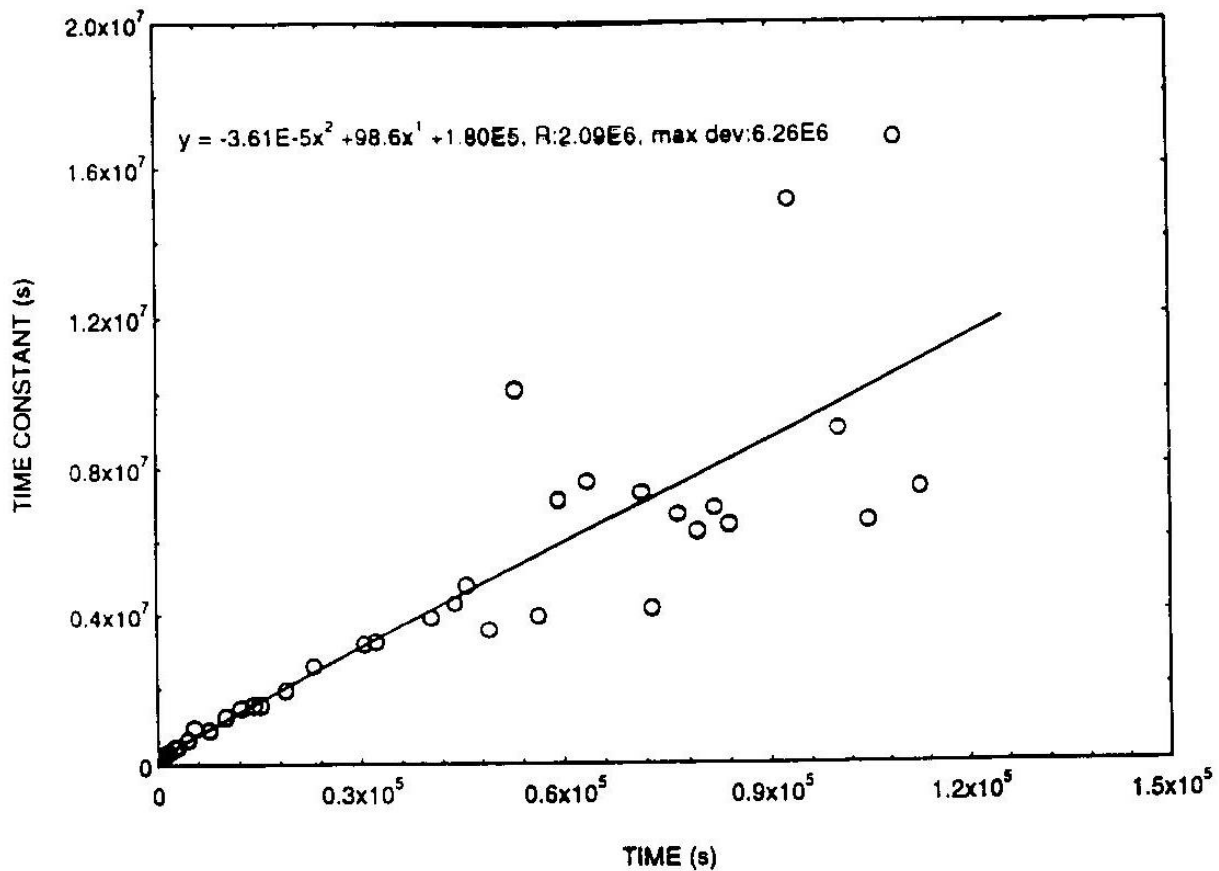


Figure 8. Time constant as a function of time for the decay shown in Figure 7.

The case of the two superconducting tubes were tested next, as an approximation to a full monolith. After charging, the tubes were kept at 4.2K by replenishing periodically the liquid helium. The field was monitored for long periods of time in order to determine the field creep.

Figure 9 shows the both fields in the bore of the innermost tube and in-between tubes. The innermost cylinder experienced a large amount of noise. We have repeated the experiment, and at the present time we think that the noise is not due to the superconducting tubes. Additional evidence is that the noise is not present at the times when the other magnets at the Laboratory were not operating.

The outer tube experiences a substantial loss in current during the duration of the experiment. The inner tube experiences a field loss very similar to that in the outer tube. The current in the inner tube is constant, while that in the outer tube is slowly decreasing. If the current in the inner tube is not at critical state, then the current in the inner tube would increase as the current in the outer tube decreases. Indeed, in the case when in the inner is not in the critical state we have observed the current in the inner tube increases as the outer tube current decreases.

The field decays by about 10%. The amount of field decay is not unreasonable, considering that during these experiments we were able to charge the outer tube to its most impressive performance (1.6T from a single tube).

The decay rate of the double tube is more complex than that of the 25 and 50 mm tubes when tested separately. We studied the effect of field decay away from critical by allowing the tube to warm up to about 18 K, with a current decrease of about 20%. At that point, liquid helium was reintroduced in the dewar, with the effect that the critical current is now about 20% larger than the current in the magnet. The decay of the field was then measured for a period of about 20 hours, at which time we ran out of liquid helium. There was no observable decay of the field during this time, indicating decay rates in excess of 40 years.

The magnet was allowed to warm up by not refilling the cryogenic coolants. The warm up process was slow enough so that the tubes were at approximately the same temperature.

The tubes were relatively small, and thermal gradients across them should be small, although they were not measured.

The critical self field as a function of temperature is shown in Figure 9. Both the inner and the outer fields are shown in the figure.

As in the cases with single tubes, the tubes does not quench as the temperature increases and the critical current is reached. Instead, the tube currents gently decrease as the temperature continues to increase. The field on the inner tube was about 2 T at 20 K.

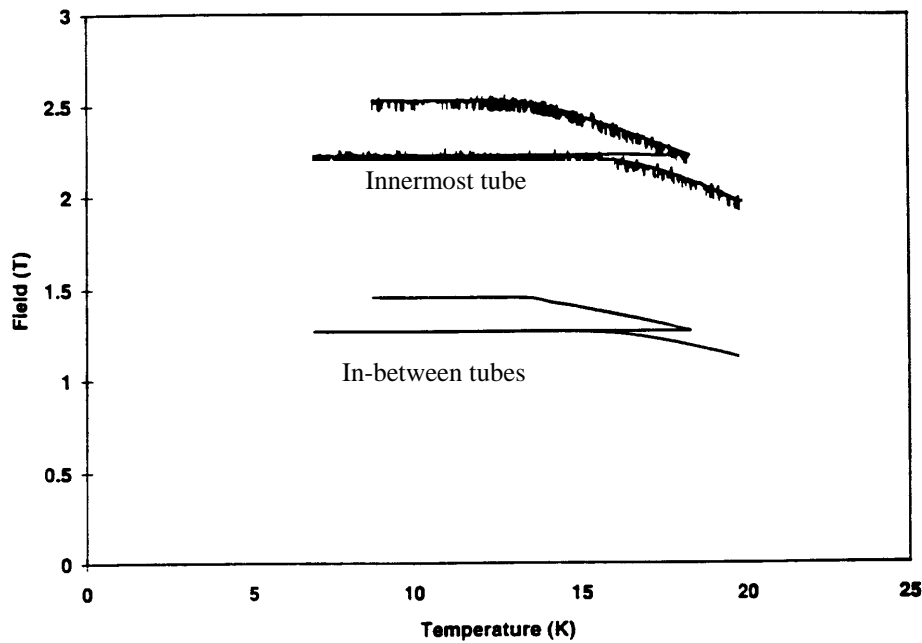


Figure 9. Magnetic field dependence as a function of temperature and time. Recools are shown.

The field in the innermost tube, after the recool from 15 K, is shown in Fig 10, vs time. There is a lot of noise, not untypical of instrumentation in the old magnet lab at MIT. There is no noticeable decay of the field, over a period of about 80000 s (over 20 hours).

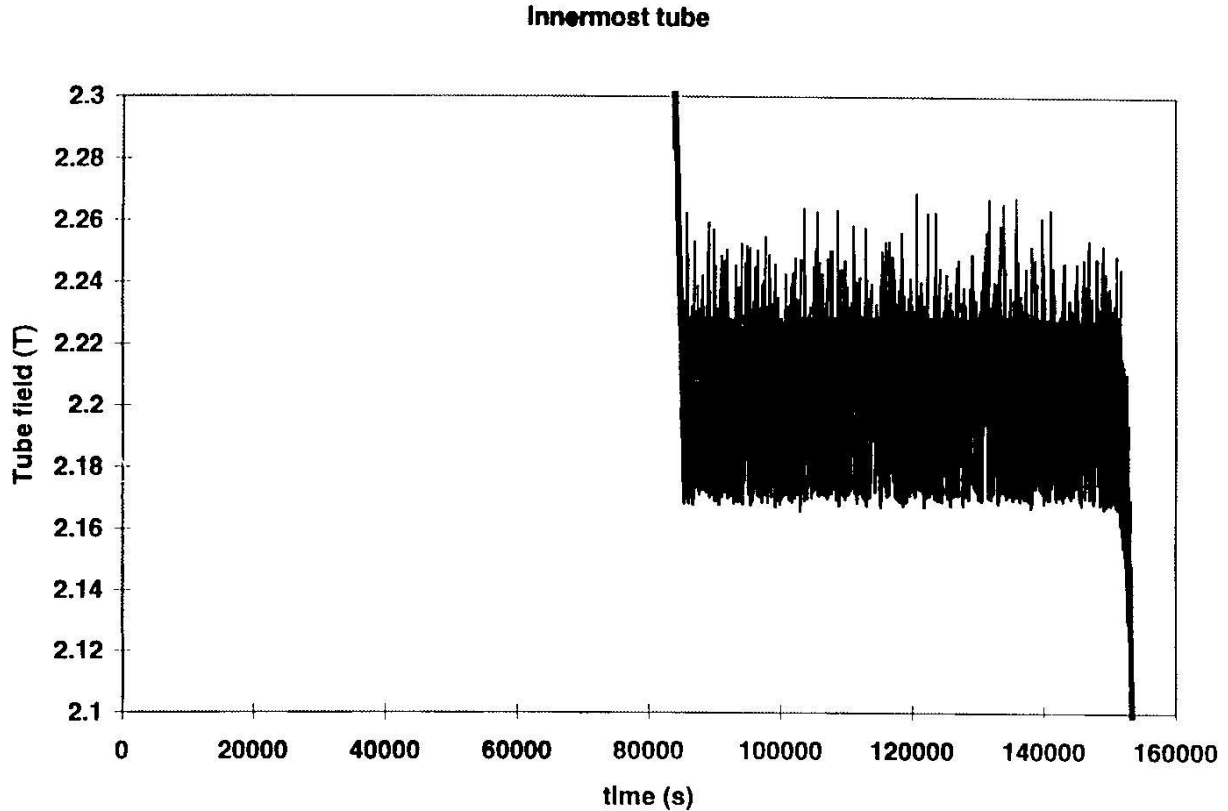


Figure 10. Field stability vs time in the innermost tube, after recool of magnet.

D. *Magnetic Field Uniformity*

Fig. 11 shows the profile of the field when the 25 mm tube was charged to 5 T and then very slowly reduced to 0. Also shown in the figure is the calculated field profile assuming an uniform current density of 200 MA/m². The current density in the magnet was actually slightly larger than 200 MA/m². The field near the tube ends is larger than would be the case for a tube with constant current density. Since the magnetic field in the tube ends is smaller than that in the middle, then the critical current density in the ends is larger than in the middle. The tube seems to have been charged in such a way that the superconductor is everywhere at its critical current. This situation is ideal, in that it maximize the utilization of the superconducting material. The other method of charging, namely applying the field and then decreasing the temperature of the tube, does not end up in a state where all the superconductor is at critical conditions. We have utilized mainly this method for charging the magnets .

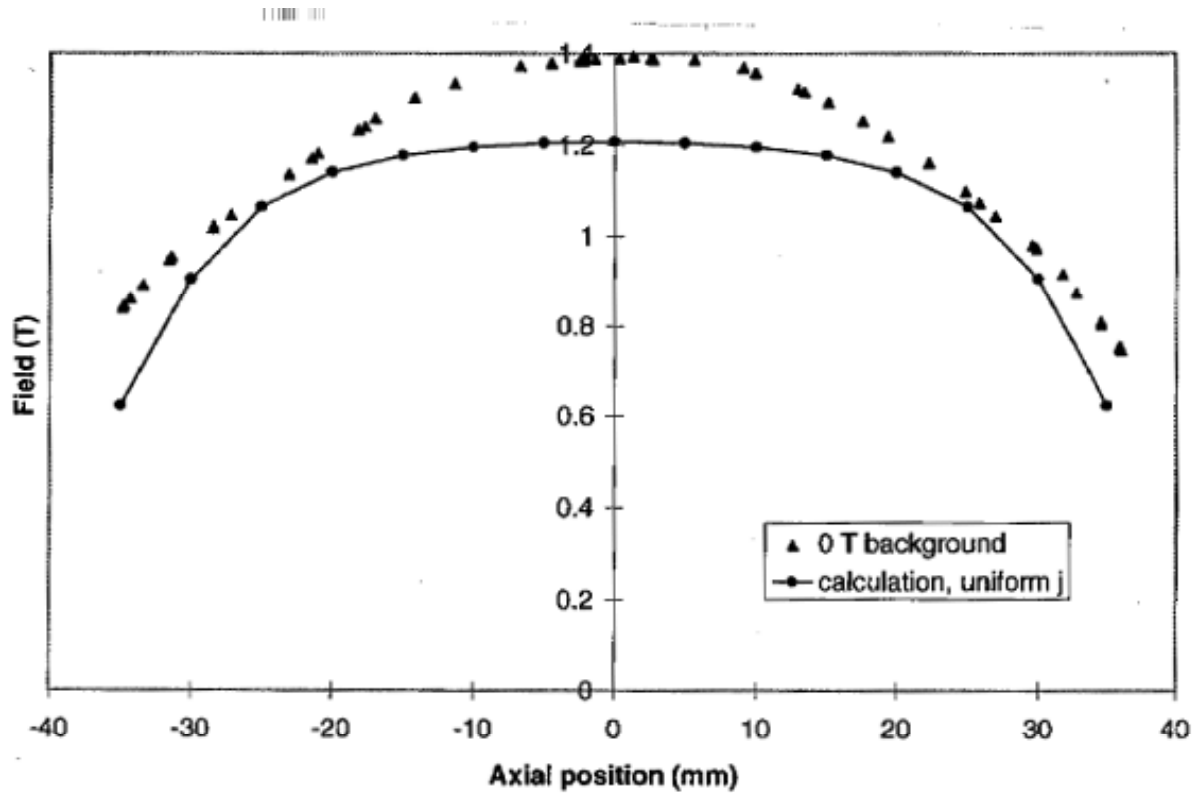


Figure 11. Axial field as a function of axial position, single 50 mm tube.

The field distribution was very different from that of the charging field. This part of the program was the most disappointing of the effort. It is clear that the monolithic approach is not going to provide the field quality required for the NMR magnets or stellarator field shaping.

VI. RADIATION DAMAGE OF HTS

The radiation damage of HTS is still a topic of active interest. Recent data indicates that the radiation damage is not worse than those of low temperature superconductivity.

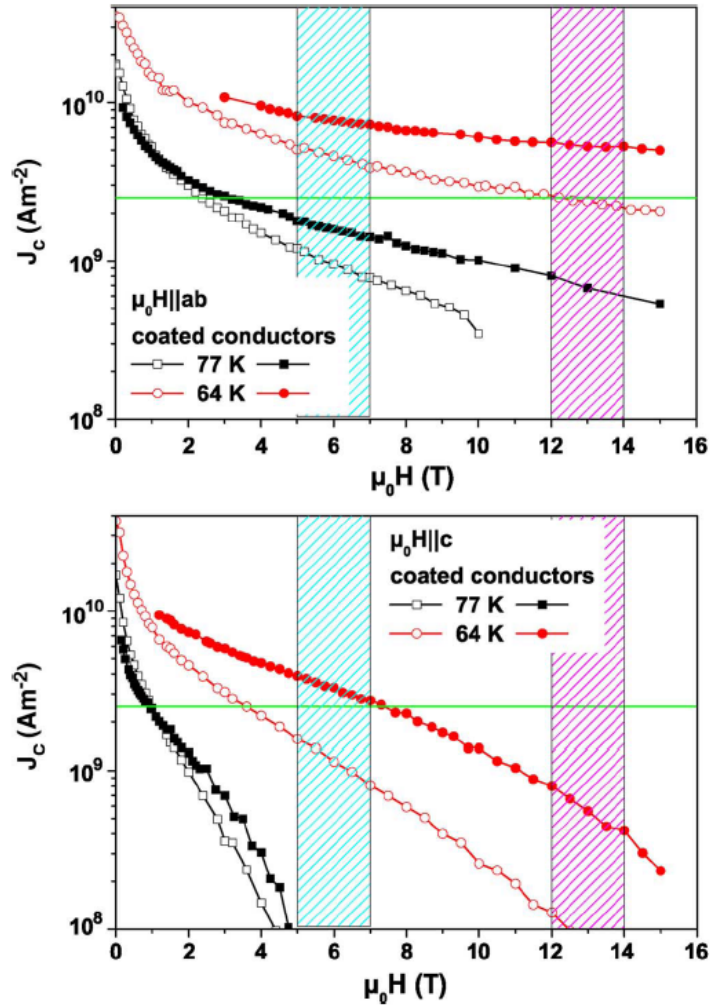


Fig 1. Critical current densities at 64 K and 77 K. Open and solid symbols refer to the worst and best samples. Critical currents for the field parallel to the ab planes (top) and to the c-axis (bottom).[From Fuger]

The coated conductors (2nd generation YBCO materials) have been characterized by Fuger et al. to doses less than $2 \cdot 10^{22}$ neutron/m² (energy greater than 0.1 MeV). The properties (at least, the current carrying capacity) peak at around $5 \cdot 10^{21} - 1 \cdot 10^{22}$ n/m², as shown in Figure 1.

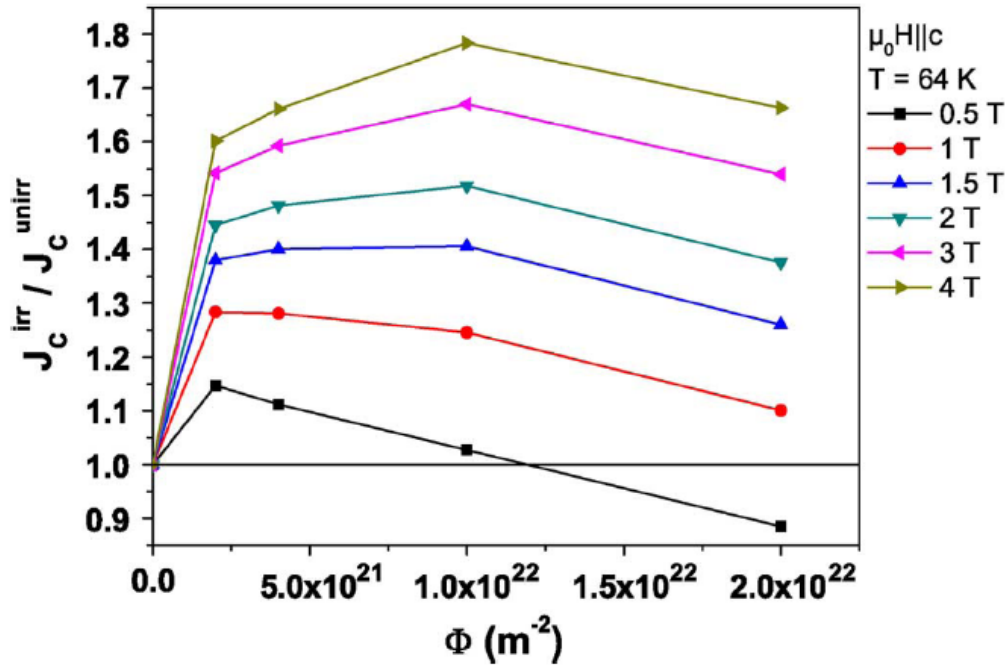


Figure 2. Ratio of the critical current density before and after irradiation to various fluences. [From Fuger]

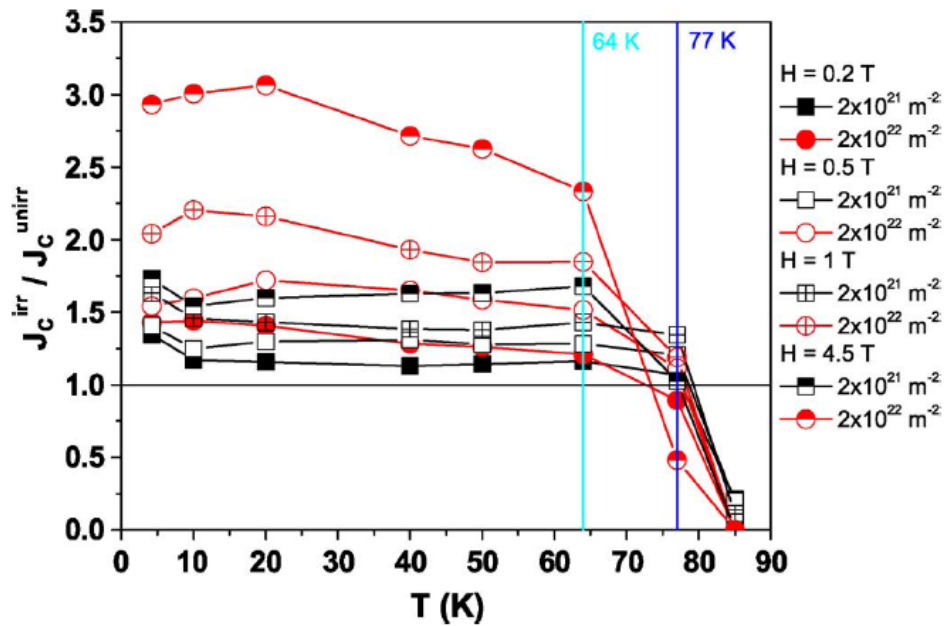


Figure 3. Increase of the critical current density as a function of temperature at different magnetic fields and neutron fluences. [From Fuger]

The coated conductors were irradiated to a fast neutron fluence of $2 \times 10^{22} \text{ n/m}^2$, i.e. two times the ITER design fluence. No degradation of the superconducting properties was observed in the relevant field and temperature range up to this fluence. At higher fluences the material starts to degrade at around 77 K [Fugen]

Not shown in the above figures is the impact on the critical temperature, as it relates to the temperature margin. Previous results suggest that the limit on the radiation is at a few times 10^{22} n/m^2 , maybe 10^{23} n/m^2 .

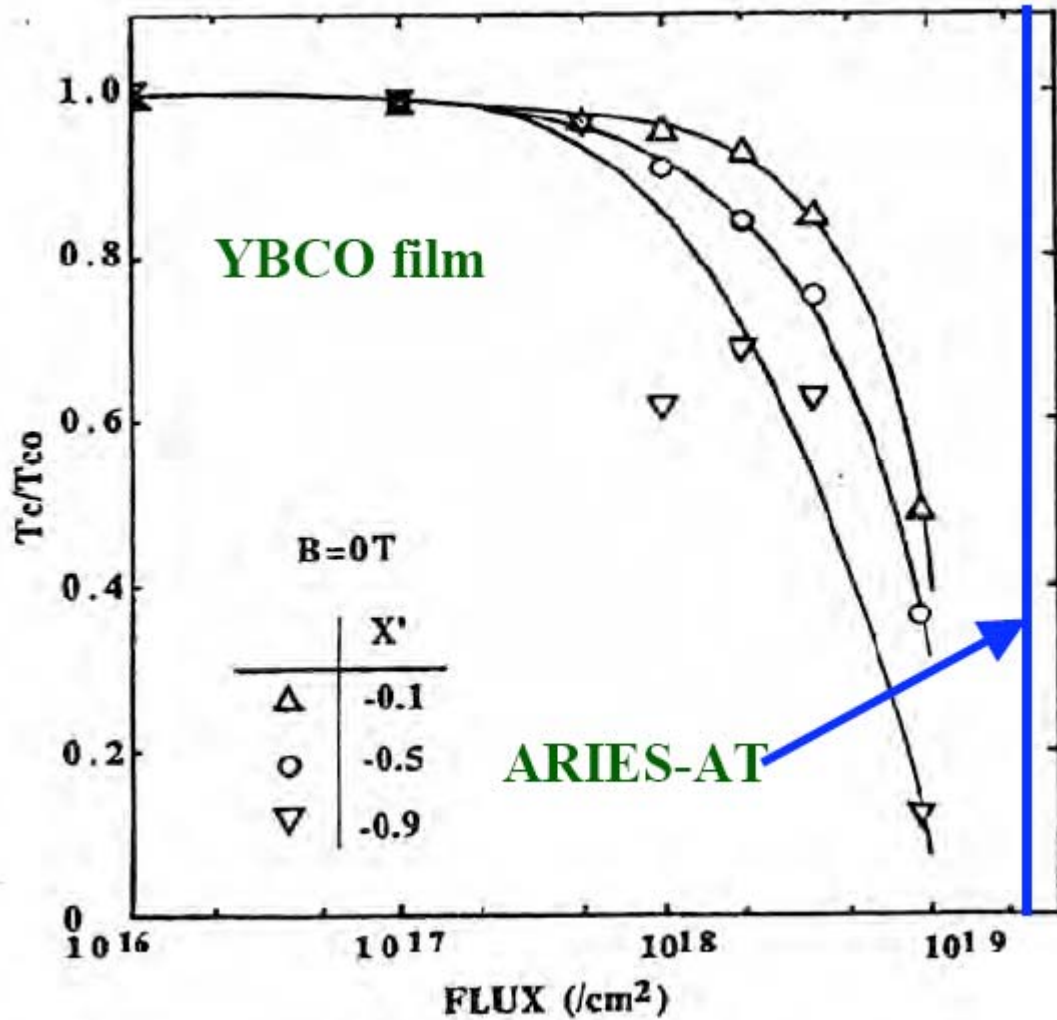


Figure 4. Ratio of critical temperature after irradiation (neutrons with energy > 0.1 MeV).

ACKNOWLEDGMENT

The suggestions and feedbacks of Michael Zarnstorff, Allan Boozer and Hutch Neilsen are appreciated.

REFERENCES

- [1] M. Tomita and M. Murakami, “*High-temperature superconductor bulk magnets that can trap magnetic fields of over 17 tesla at 29 K*”, *Nature* **421** 517 (2003)
- [2] M. Tomita, M. Murakami, K. Itoh and H. Wada, *Mechanical properties and field trapping ability of bulk superconductors with resin impregnation*, *Supercond. Sci. Technol.* **17** (2004) 78–82
- [3] Frank N. Werfel, Adelwitz Technologiezentrum GmbH (ATZ), private communication (2009)
- [4] Achim Hobl, Nexans Superconductors, private communication (2009)
- [5] Y. Kimura, K. Yamaguchi, T. Sano, *et al.*, *Practical Technique of Pulsed Field Magnetization for Bulk HTS Application*, *J. Physics, Conference Series* **97** (2008) (8th European Conference on Applied Superconductivity)
- [6] A.H. Boozer (Columbia University), Neil Pomphrey and Art Brooks, *Tokamak toroidal field coils with open access to the plasma chamber*, manuscript in preparation (2009), New York
- [7] A.H. Boozer, *Magnetic Shielding Using Small Pieces of Superconductor*, manuscript in preparation (2009)
- [8] L. Bromberg, *Methods of charging superconducting materials*, US Patent 6621395
- [9] D.R. Cohn, L. Bromberg *et al.*, *Microwave/far infrared cavities and waveguides using high temperature superconductors*, US Patent 5231073
- [10] D.R. Cohn, L. Bromberg *et al.*, *Microwave/far infrared cavities and waveguides using high temperature superconductors*, US patent 4918049
- [11] Beidler, C.D., E. Harmeyer, F. Herrnegger, *et al.*, The Helias reactor HSR4/18, *Nuclear Fusion*, 41, No. 12, (2001) 1759
- [12] Sagara, A., Motojima, O., LHD-type reactor design studies, *Fusion Technology*, 34, n 3, pt.2, Nov. 1998, p 1167-73

- [13] Wanner, M., J.-H. Feist, H. Renner, J. Sapper, F. Schauer, H. Schneider, V. Erckmann, H. Niedermeyer, W7-X Team, Design and construction of WENDELSTEIN 7-X, *Fusion Engineering and Design* 56–57 (2001) 155–162
- [14] Komori, A., Yamada, H.; Kaneko, O. et al., Overview of the Large Helical Device, *Plasma Physics and Controlled Fusion* 42, n 11, Nov. 2000, p 1165-77
- [15] Konrad Risse, Th. Rummel, L. Wegener et al., Fabrication of the superconducting coils for Wendelstein 7-X, *Fusion Engineering and Design* 66 /68 (2003) 965 /969
- [16] E. Harmeyer, J. Kißlinger, Improved support concept for the Helias reactor coil system, *Fusion Engineering and Design* 66 /68 (2003) 1025 /1028
- [17] Jaksic, N., J. Simon-Weidner, J. Sapper, Final structural and mechanical evaluation of the W7-X magnet support system, *Fusion Engineering and Design* 58–59 (2001) 259–263
- [18] Neilson, B.E., L.A. Berry, A. Brooks et al., Design of the National Compact Stellarator Experiment (NCSX), *Fusion Eng. & Des.* 66-68 (2003) 169-174.
- [19] Williamson, D., Brooks, A., Brown, T. et al., Modular coil design developments for the National Compact Stellarator Experiment (NCSX) *Fusion Engineering and Design*, 75-79, Nov. 2005, p 71-4
- [20] Bromberg, L., J.H. Schultz, L. El-Guebaly *et al.*, *High Performance Superconducting Options For Aries Compact Stellarator*, submitted for publication to *Nuclear Fusion and Technology* (2008)
- [21] R. Fuger, M. Eisterer, and H.W. Weber, *YBCO Coated Conductors for Fusion Magnets*, *IEEE Transactions Applied Superconductivity*, accepted for publication